A physics-forced spatial Ecopath with Ecosim model reproduces spring bloom timing in the Strait of Georgia

Greig Oldford[1,2], Brian Hunt[1], Carl Walters[1], Villy Christensen[1,3]

[1] Institute for the Oceans and Fisheries, University of British Columbia, Vancouver, BC, Canada
[2] Science Branch, Fisheries and Oceans Canada, Vancouver, BC, Canada
[3] Ecopath International Initiative, Barcelona, Spain

Corresponding author: Greig Oldford (greig.oldford@dfo-mpo.gc.ca)

Abstract

Marine ecosystem models rarely simulate lower trophic level (LTL) production from physical conditions; production is usually prescribed or supplied by a separate biogeochemical model. We tested whether Ecopath with Ecosim (EwE) can reproduce physically controlled LTL dynamics without a dedicated biogeochemical model. The Strait of Georgia Ecosystem Model of Lower Trophic Levels (SOGEM-LTL) represents 22 pelagic functional groups in the Strait of Georgia, Canada, with simplified nutrient dynamics, and is forced offline by a physical-oceanographic hindcast and an atmospheric reanalysis. We ran it from 1980 to 2018 at a three-day timestep and evaluated it against observations of spring bloom timing, phytoplankton, dissolved inorganic nitrogen and zooplankton. Interannual variation in bloom timing emerged from the physical forcing: the spatial (Ecospace) configuration matched satellite-derived bloom timing ($r = 0.77$, mean absolute error 10.5 days) and its early, average or late category in 13 of 14 years, more closely than a non-spatial (Ecosim) configuration of the same food web (10 of 14). The model also reproduced the seasonal cycles of nitrogen drawdown and recovery and of crustacean zooplankton biomass. Simulated variability was generally lower than observed, and skill was higher for seasonal and phenological indicators than for point-to-cell biomass comparisons. SOGEM-LTL sits between one-dimensional bloom models and three-dimensional biogeochemical models, adding trophic resolution at low computational cost and provides a basis for end-to-end models that link ocean physics to fish through their prey.

Keywords: Ecopath with Ecosim; Ecospace; spring bloom phenology; lower trophic levels; zooplankton; Strait of Georgia

1. Introduction

Ocean conditions shape the timing and magnitude of plankton production, and with it the food available to fish and other consumers (Cushing, 1971; Friedland et al., 2012; Gargett, 1997; Kiørboe, 2018; Ratnarajah et al., 2023; Stenseth et al., 2002; Suchy et al., 2022). Linking changes in fish productivity to ocean conditions is nonetheless difficult: observations are sparse, dynamics are nonlinear, and the drivers cannot be manipulated experimentally. Models that carry physical forcing through the food web can help, but the two modelling traditions best placed to do so each capture only part of the zooplankton link (Mitra et al., 2014; Ratnarajah et al., 2023). Biogeochemical models simulate production from physical forcing but usually reduce zooplankton to one or two groups that act mainly as a closure term, and their dynamics are sensitive to how that term is formulated (Chenillat et al., 2021; Omta et al., 2023). Food-web and fisheries models resolve consumers in detail but usually take plankton production as an input, from observations or from biogeochemical and Earth-system models, and their projections depend on which input is used (Heneghan et al., 2021; Kearney et al., 2021). Yet fish catch varies far more among ecosystems than primary production does, and much of that difference is explained by how energy passes from phytoplankton to fish (Stock et al., 2017). In both modelling traditions, this bridge between physics and fish is the least constrained part of the model (Mitra et al., 2014; Petrik et al., 2022).

Three-dimensional biogeochemical models that connect physical, chemical and ecological dynamics are computationally demanding for multi-decadal, ensemble or scenario applications (Libralato and Solidoro, 2009; Rose et al., 2010), so one approach is to reduce process detail while maintaining predictive skill (Hannah et al., 2010; Martin et al., 2024). Ecopath with Ecosim (EwE) is a widely used candidate for such reduced-complexity, end-to-end (E2E)

applications, but in most EwE applications, which focus mainly on fish and fisheries (Colléter et al., 2015; Morales-Zárate et al., 2026), primary production is prescribed through forcing functions, sometimes derived from observed environmental time series (Oka and Sohma, 2026), or supplied by a biogeochemical model coupled online or used as offline forcing (Akoglu et al., 2015; Araignous et al., 2026; Coll et al., 2020; de Mutsert et al., 2016; Dişa et al., 2024). Whether EwE alone can reproduce physically controlled LTL dynamics, such as the timing of the spring bloom, has not been deeply explored. Here, we investigate whether EwE (Christensen and Walters, 2024) can reconstruct intra-annual LTL dynamics, particularly the Ecospace module (Walters et al., 1999) forced offline by a physical-oceanographic hindcast and atmospheric reanalysis (Oldford et al., 2025). Doing so requires transparent evaluation of where such models are skillful and what their limits are (Fulton et al., 2019; Steenbeek et al., 2021; Susini and Todd, 2021).

Our case study, the Strait of Georgia (SoG), is a semi-enclosed estuarine sea in the northeast Pacific (Figure 1) that has experienced gradual and abrupt physical and ecological change since the late 1970s (Johannessen and Macdonald, 2009; Perry and Masson, 2013; Riche et al., 2014). Spring bloom timing has become more variable, with the potential to alter the temporal alignment of phytoplankton, zooplankton and their predators (Allen and Wolfe, 2013; Cushing, 1990; Suchy et al., 2022). Bloom timing in the SoG is controlled mainly by wind-driven mixing and light, has been hindcast with a one-dimensional model back to 1968, and has been estimated from satellite observations since 2003 (Allen and Wolfe, 2013; Collins et al., 2009; Suchy et al., 2022). Bloom timing is thus a candidate seasonal ecological indicator to help test whether physical forcing propagates correctly through a food-web model. Regime shifts and interdecadal variability have been linked to the productivity of fish stocks (Beamish et al., 2004, 1999;

Coronado and Hilborn, 1998; Hare and Mantua, 2000; Perry and Masson, 2013; Sobocinski et al., 2021) and to declines in the early marine survival of juvenile Coho and Chinook salmon (Pearsall et al., 2021; Ruff et al., 2017; Zimmerman et al., 2015). Changes in the timing, composition and biomass of LTL prey fields may contribute to these declines and to variation in Pacific herring productivity (Boldt et al., 2025; Pearsall et al., 2021). Observations alone are insufficient to reconstruct how production and prey phenology have varied across the SoG over these decades.

We developed the Strait of Georgia Ecosystem Model of Lower Trophic Levels (SOGEM-LTL), representing 22 pelagic functional ecological groups. We evaluated its 1980–2018 hindcast against observations of bloom timing, phytoplankton, nutrients and zooplankton. We asked three questions: (1) Does interannual variation in spring bloom timing emerge in EwE when primary production responds directly to physical-oceanographic and atmospheric forcing, without a dedicated biogeochemical model? (2) Does spatial resolution improve the representation of bloom timing relative to a non-spatial configuration of the same food web? (3) Do the seasonal cycles of nutrients, phytoplankton and crustacean zooplankton prey follow the observations, and which of these indicators does the reconstruction represent most reliably for fisheries and ecosystem applications?

2. Methods

2.1 Framework and application

EwE is a widely used marine ecosystem modelling framework (Colléter et al., 2015) composed of three nested sub-models: Ecopath (a static mass-balanced trophic model), Ecosim (a non-spatial time-dynamic extension), and Ecospace (a spatially and temporally explicit

implementation; 2-D). Each module has a set of core parameters with associated structural equations summarised in the Supplemental Material (Section S.1; Table S1). We use the Windows desktop version 6.7 (Christensen and Walters, 2024). Detailed descriptions of the framework, equations, and plugins are available elsewhere (Christensen and Steenbeek, 2024; Christensen and Walters, 2024), and the configuration used here is described below.

SOGEM-LTL v1 includes three primary producer groups, three mixotrophic groups ('protozooplankton'), five crustacean zooplankton groups, four soft-bodied (gelatinous) groups, one ichthyoplankton group, three nekton groups, one bacterial group, and two detrital groups (Figure 2). Functional groupings (Table S2; Table 1) were chosen based on several considerations including body size, taxonomy, and trophic role. Groupings were chosen to represent size structure, gelatinous groups, and microbial loop pathways (Section S.2.2). The parameterisation was informed by local field observations where available; otherwise, other models or empirical relationships were used to inform the initial parameterisation. Fisheries were not included because a follow-up model representing upper trophic levels and fisheries is under development. Basic Ecopath parameters are listed in Table 2, the balanced food web is shown in Figure 3, and the main configuration settings are summarised in Table 3; further details of the parameterisation, including biomass, diet, size-class, vulnerability settings, and accompanying sources and rationale are provided in Section S.2 of the Supplemental Materials (Tables S3–S18).

A regular horizontal grid based on the NEMO-based Hindcast of the Salish Sea v1 (HOTSSea; Oldford et al., 2025) was used, with an approximately 1.5 km grid spacing, rotated 29° anti-clockwise along the axis of the SoG, clipped to exclude Puget Sound and the Juan de Fuca Strait to focus on the SoG (Figure 1); forcing was masked near the Fraser River mouth, where turbidity

could not be estimated reliably (Section S.2.8.3). Our model uses carbon as currency, chosen primarily for consistency with previous models and to minimize conversion-related error when evaluating against in situ measurements.

Physical fields from HOTSSea and from the Regional Deterministic Reanalysis System atmospheric reanalysis, RDRS v2.1 (Gasset et al., 2021), were used to provide external physical forcings. A custom software framework was used to link Ecosim and Ecospace to the forcings in an 'offline' manner, by reading pre-processed files from the physical ocean and atmospheric models (Figure S2). The framework also includes sub-models for 3-D to 2-D pre-processing and for converting 2-D shortwave radiation to photosynthetically active radiation (PAR) integrated over the euphotic zone (Section S.2.6). Therefore, in the present implementation, coupling is one-way: physical and atmospheric fields force the biological model, but biology does not feed back on circulation, stratification, or mixing. Descriptions of the forcing fields and the 3-D to 2-D conversion are provided in Section S.2.3 (Figure S1) and the associated data (Oldford, 2026a) and code (Oldford, 2026b) are archived on Zenodo.

2.2. LTL representation

Primary Production

In the Ecosim and Ecospace modules, primary productivity is modelled as the product of three functions representing (1) intra-group or inter-group inhibition (non-specific), (2) nutrient limitation, and (3) environmental conditions, in addition to an optional primary production multiplier, P_{mult}:

$$\mu_t = \underbrace{f(B_t, B_{t=0}, \mu_{max})}_{\substack{biomass,\\ shading,\ self-limitations}} \times \underbrace{f(N_f)}_{nutrient\ effects} \times \underbrace{\prod_{i=1}^{n} f_i(env_i)}_{\substack{environmental\\ effects}} \times \underbrace{P_{mult}}_{\substack{primary\\ production\\ multiplier}} \quad \text{Eq. 1}$$

where μ_t is population growth rate at time, *t*, (i.e., equivalently Ecopath's *P/B* under equilibrium), B_t is phytoplankton biomass, $B_{t=0}$ is the base Ecopath biomass, μ_{max} is the maximum phytoplankton growth rate, *N* represents nutrients (non-specific), and *env* represents one of a possible collection of environmental response functions (range: 0-1). To represent the limitation of growth due to factors like self-shading and other self-limiting effects, productivity is assumed to be inversely proportional to biomass:

$$f(B_t, B_{t=0}, \mu_{max}) = \frac{\mu_{max}}{1+B_t h} \quad \text{Eq. 2}$$

where the maximum growth rate, μ_{max}, is parameterised based on an estimate of the ratio of initial growth rate, $\mu_{t=0}$, to a user-set maximum possible growth rate (Christensen and Walters, 2024, 2005). The *h* term represents a scalar that is based on the relative realized growth at the initial biomass:

$$h = (\frac{\mu_{max}}{\mu_{t=0}} - 1)/B_{t=0} \quad \text{Eq. 3}$$

A parameter representing the maximum production relative to the initial conditions, $\mu_{max\text{-}r}$, is used to calculate μ_{max}, including effects on productivity attributed to intra-group inhibition (e.g., self-shading, allelopathy).

Primary production in SOGEM-LTL was parameterised to be controlled by light and nutrients, with moderate turbulence typical of the transition from winter to spring particularly important for bloom-forming diatoms (Gargett, 1997; Li et al., 2000). The PP1-DIA group, representing diatoms, was parameterised based on the hypothesis that high division rates under high-nutrient

and moderately turbulent conditions are the primary mechanism enabling the seasonal dominance of this group. While bloom onset in many regions aligns with the mixed layer depth (MLD; the pycnocline or halocline; Sarmiento and Gruber, 2006), strong tidal mixing and freshwater buoyancy input in the SoG continuously disrupt simple stratification patterns (Collins et al., 2009). A more useful indicator than MLD may therefore be the depth of the turbulence-defined mixing layer (XLD, i.e., "turbocline"; Allen and Wolfe, 2013; Behrenfeld and Boss, 2014; Franks, 2015; Huisman et al., 2004, 1999). We therefore used XLD from HOTSSea to help calculate the irradiance received by phytoplankton (Figure S2).

Environmental responses

Environmental responses can be parameterised in Ecosim and Ecospace to help represent environmental effects on growth, consumption, foraging, and mortality of functional groups (Christensen et al., 2014). Using a spatiotemporal framework built for the Ecospace module (Steenbeek et al., 2013), external spatiotemporal data were assimilated at each timestep. The spatiotemporal driver data were then combined with the defined environmental responses to determine the overall response of a given functional group to environmental factors.

Photosynthesis-irradiance (PI) responses were parameterised in SOGEM-LTL for each autotrophic and mixotrophic group as environmental responses to irradiance, scaling growth according to PAR. We adopted a simple structure that yields a Blackman-like shape (Aalderink and Jovin, 1997; Jassby and Platt, 1976), convenient in its simplicity and because it corresponds to the built-in EwE 'right-shoulder' response:

$$\mu(I) = \begin{cases} \alpha I, & I < I_{opt} \\ 1, & I \geq I_{opt} \end{cases} \quad \text{Eq. 4}$$

where $\mu(I)$ is the 'environmental response' [0,1] to irradiance. Assuming growth is zero in complete darkness and thus $\alpha = 1/I_{opt}$ only the I_{opt} parameter (W m^{-2} of depth-integrated PAR) is required. The EwE 'right-shoulder' setup requires three parameters with the 'right point' parameter corresponding to I_{opt}. Further details are provided in Section S.2.7 (Tables S23–S24).

Temperature control on phytoplankton growth was parameterised using a custom response based on a piecewise Gaussian thermal performance curve:

$$\mu(T) = \begin{cases} \exp\left(-a\left(T - T_{opt}\right)^2\right), & T \leq T_{opt} \\ \exp\left(-b\left(T_{opt} - T\right)^2\right), & T > T_{opt} \end{cases} \quad \text{Eq. 5}$$

where T is temperature (°C), T_{opt} the cardinal optimum, and a and b (°C^{-2}) independently set the cold-side and warm-side curvature, respectively. This formulation is similar to the one used in other regional models (Khangaonkar et al., 2021, 2012) and retains a useful relationship between the cold-side tuning parameter, a, and reported Q_{10} when it is defined relative to the optimum (e.g., Anderson et al., 2021), where:

$$Q_{10} = \frac{f(T_{opt})}{f(T_{opt} - 10°\mathrm{C})} = e^{a(10°\mathrm{C})^2} \;\rightarrow\; a = \ln(Q_{10})/(10°\mathrm{C})^2 \quad \text{Eq. 6}$$

The structure captures the empirically observed rise to an optimum followed by a decline at high temperature. For heterotrophs, cardinal temperatures (T_{min}, T_{opt}, T_{max}) describing thermal niche envelopes are often all that is available in the literature (e.g., Kaschner et al., 2023), which can be accommodated:

$$a = -\frac{\ln(\varepsilon_1)}{(T_{opt} - T_{min})^2} \quad \text{Eq. 7}$$

and

$$b = -\frac{\ln(\varepsilon_2)}{(T_{max} - T_{opt})^2} \quad \text{Eq. 8}$$

where ε_1 and ε_2 are the relative responses (0–1) at T_{min} and T_{max}, respectively. The parameterisation with respect to zooplankton and the parameters used for all groups are provided in Section S.2.7 (Tables S25–S29; Figure S3).

Nutrients

EwE represents a simplified nutrient cycle in which a single generic nutrient constrains primary production, while the redistribution of nutrient between free and bound forms is driven by changes in biomass and external nutrient inputs (optionally). To represent the effect of nutrient limitation on primary production, the framework's nutrient formulation partitions a single generic nutrient pool into a free component and a component bound in biomass. Total nutrient is therefore treated conceptually as:

$$N_{\text{tot}} = N_{\text{free}} + N_{\text{bound}} \quad \text{Eq. 9}$$

where N_{free} denotes nutrients available for uptake and N_{bound} denotes nutrients incorporated into living biomass and other organic pools. In this formulation, nutrients are handled implicitly through mass balance and mediation of production; the model does not track a prognostic dissolved nutrient state variable in the same manner as a full biogeochemical model. Initial conditions are specified through the proportion of total nutrient that is free:

$$p_{\text{free}} = \frac{N_{\text{free}}}{N_{\text{free}} + N_{\text{bound}}} \quad \text{Eq. 10}$$

which determines how the total nutrient inventory is partitioned at the start of the simulation. In its simplest form, this representation treats the nutrient pool as a single generic currency and applies nutrient limitation broadly across primary producer groups rather than resolving multiple

nutrients or group-specific internal stoichiometry. Primary production is then coupled to nutrient availability through a saturating function referenced to the initial free nutrient inventory (Christensen and Walters, 2024):

$$f(N_f) = \frac{2N_{f,t}}{N_{f,t}+N_{f,t=0}} \quad \text{Eq. 11}$$

Using this formulation, free nutrients may increase relative to the initial condition and producer growth rates may accordingly increase by a maximum factor of two. The nutrient multiplier is equivalent to a scaled Michaelis–Menten function in which the half-saturation constant is set equal to the baseline nutrient concentration, consistent with the expectation that natural selection adjusts half-saturation constants relative to ambient nutrient concentrations (Crowley, 1975).

For the SOGEM-LTL parameterisation, nitrogen was adopted as the reference nutrient for parameterisation because dissolved inorganic nitrogen is generally considered the macronutrient limiting phytoplankton production in the SoG (Harrison et al., 1983; Olson et al., 2020), although other nutrients, including silica and iron, may become limiting at certain times. Effort was made to parameterise SOGEM-LTL to represent surface waters that become seasonally replenished with nutrient-replete deeper water, followed by nutrient drawdown during spring and summer due to uptake by primary producers and increased stratification. At the scale of the SOGEM-LTL domain, terrestrial nutrient inputs are relatively minor compared with marine sources (Mackas and Harrison, 1997; Sutton et al., 2013). Accordingly, the initial free fraction was parameterised from observed nitrate plus nitrite inventories in the upper 20 m of the water column (Fisheries and Oceans Canada, 2025; Pacific Salmon Foundation (PSF), 2025). Additional details on the data sources, calculations, and rationale are provided in Section S.2.4 (Table S19).

Because the EwE framework does not explicitly resolve vertical water-column structure, seasonal nutrient resupply was represented with Ecosim's 'nutrient-loading function', driven by an empirical proxy derived from the HOTSSea model's XLD field, which varies in response to wind, tides, buoyancy forcing, and estuarine circulation. Within Ecospace, spatial variation in this effect was represented using the standard 'relative primary productivity' map, with normalized spatial forcing maps derived from the same XLD fields and applied across the model domain. Thus, in both modules, XLD was used as an empirical proxy to address the issue of moving from 3-D to 2-D while representing the process of nutrient resupply to the productive surface layer.

Detrital pathways

Two detrital groups were included in the model: the DE1-POC group represents particulate organic carbon (POC) and the DE2-DOC group represents dissolved organic carbon (DOC). Flow to each detrital group was parameterised specifically for each ecological functional group. Total detritus was distributed evenly between the two detrital pools, given a lack of data to use to better differentiate.

SOGEM-LTL omits much of the upper trophic levels, which would divert a portion of flows away from immediate detrital pathways. Detrital flows from the top trophic levels in this truncated model would therefore be overestimated. Using a previously developed organic carbon budget (Johannessen et al., 2003), we estimated that roughly one-third of new production is exported rapidly from the photic zone as POC and is either buried or oxidized within sediments or in the water column. A portion of the detrital flux from these groups was therefore adjusted to be sent to export. Further details of the model parameterisation with respect to detritus are provided in Section S.2.5 (Tables S20–S22).

2.3. Numerical configuration and calibration

Temporal configuration

EwE uses 12 timesteps per model time unit; by default, rates are annual and the timestep is monthly. We treated each model unit as one-tenth of a calendar year and multiplied annual rate parameters by 0.1, giving 120 intervals per calendar year, each approximately three days long. Days 1–357 were divided into 119 consecutive three-day blocks, and the final block covered the remaining days (days 358–365, or 358–366 in leap years). All forcing fields were converted using the same mapping. The choice of temporal resolution balanced several considerations, including resolving bloom dynamics, the desire to use a consistent numeric integration scheme across functional groups, and working within the software's simulation limit of 500 years (i.e., maximum 500 model time units would equate to a 50-year hindcast in the present setup). The 1980–2018 Ecospace hindcast, run multithreaded, required approximately 35 minutes including output writing on a desktop computer (AMD Ryzen 9 7900X, 12 cores, 32 GB DDR5 RAM).

Spin-up

Two modifications were made to account for the increased temporal resolution during Ecospace's spin-up procedure. First, climatological means of the forcing fields were used for the initial 12 timesteps, over which the framework's spin-up procedure iterates. The spin-up repeated for the equivalent of 5 years. Then, the 1980 forcing was repeated for two further years to extend equilibration, labelled "1978" and "1979", and output for those "years" was excluded from evaluation (Section S.2.8.1; Table S30).

Parameterisation and calibration sequence

The initial parameterisation followed standard steps (Christensen and Walters, 2024; Heymans et al., 2016): (i) Ecopath diagnostics of mass balance and consistency with ecological theory (Christensen and Walters, 2024; Link, 2010), with PREBAL diagnostics shown in Figure S4; (ii) configuration and calibration of Ecosim, with vulnerability multipliers kept near their default ($\gamma = 2$; lower values imply predators close to carrying capacity) and other parameters close to their defaults (Table S15); and (iii) configuration of Ecospace, with movement and dispersal parameters kept near their default values following general guidance (de Mutsert et al., 2023). Dispersal rates are given in Table S16. Model parameters were calibrated against available observations, within bounds constrained by empirical estimates, literature values, and ecological theory. Calibration was not exhaustive and most parameters were kept near their initial values. No observations were withheld for independent evaluation; reported skill metrics therefore describe calibrated hindcast performance. Zooplankton survey data (1996–2018) informed initial Ecopath biomasses and were also used for evaluation, and nitrate observations informed the initial free-nutrient fraction and were also used for evaluation; for these components, reported skill is not independent of model development. Bloom-timing series, QU39 phytoplankton counts and seasonal phytoplankton estimates were not used to set parameters, although calibration choices were made with knowledge of the bloom-timing comparison.

2.4. Evaluation design

Evaluation data and comparison design

We evaluate the calibrated hindcast against observations of (1) spring phytoplankton bloom timing, (2) intra-annual phytoplankton community variability, (3) seasonal nutrient patterns, and (4) seasonal zooplankton biomass (Table 4). Where observations also informed parameterisation

or calibration, comparisons assess calibrated hindcast performance rather than independent predictive skill. Matching, transformations, and aggregation differed among datasets as described below. Performance was assessed using bias, mean absolute error (MAE), root mean square error (RMSE), Pearson's correlation coefficient (r), and the Willmott Skill Score (WSS). Error metrics retain the units of the evaluated variable; for standardised anomalies, they are dimensionless. Equations are provided in Section S.3.2.

Spring bloom timing

Spring bloom timing was evaluated against satellite-derived estimates for the SoG reported by Suchy et al. (2022) for 2003–2016. SOGEM-LTL output was extracted from grid cells within a mask approximating the satellite analysis area. For each 3-day model timestep, total phytoplankton biomass was calculated as the sum of the diatom (PP1-DIA), nanophytoplankton (PP2-NAN), and picophytoplankton (PP3-PIC) groups. The masked field was then reduced to a single time series using the spatial median across ocean cells.

Bloom initiation was defined using a threshold rule chosen to approximate that of Suchy et al. (2022): the first date in a given year when biomass exceeded 1.05 times the annual median and was followed by sustained elevated biomass, here defined as at least two of the next four model outputs remaining above 70% of that threshold. Bloom years were further classified as early (day of year ≤ 68), average (days 69–107), or late (day of year ≥ 108), following Suchy et al. (2022). In addition to standard timing statistics, we recorded the number of years in which the model and observations agreed in bloom category. Bloom timing was also evaluated against the one-dimensional bloom-model hindcast (Allen and Wolfe, 2013; Collins et al., 2009), hereafter C09, and outputs from the non-spatial SOGEM-LTL Ecosim configuration using the same general

bloom-detection framework. Further details of the C09 and Ecosim comparisons are provided in Section S.3.3.

To illustrate seasonal and spatial phytoplankton development, Ecospace output was also compared with the 8-day MODIS-Aqua chlorophyll a composites underlying the satellite bloom series (2003–2016; Suchy et al., 2022), each source expressed relative to its own seasonal median; spatial agreement was summarised as the correlation across grid cells between the monthly maps (Section S.3.3).

Primary Productivity and Phytoplankton

The annual primary production implied by the balanced EwE parameterisation was compared to empirical estimates compiled from literature (Table S32). Seasonal phytoplankton community composition and absolute biomass estimates from a previous Ecopath model were also used for comparison (McEwan et al., 2023).

To evaluate the model's representation of phytoplankton temporal variability, 110 microscopy-based samples collected at station QU39 in the northern SoG during 2016–2018 were used (Del Bel Belluz, 2024). Because the observations were reported as cell counts and robust group-specific conversions to carbon were not available for all taxa, evaluation focused on relative temporal variability rather than absolute biomass. Species-level counts were first summed to the observational classes corresponding to the Ecospace functional groups PP1-DIA, PP2-NAN, PP3-PIC, and PZ2-DIN, and each observation was matched to the closest Ecospace grid cell and model timestep. Observed and modelled values were then log-transformed and expressed as standardised departures from the group-specific annual mean, using the standard deviation of the monthly means for normalization. Monthly distributions of the standardised departures from the annual means were compared to assess whether the model reproduced the seasonal timing and

relative magnitude of phytoplankton variability. Light microscopy does not resolve picophytoplankton, so the PP3-PIC comparison used Pyramimonadophyceae as an indicator taxon; because these prasinophytes are mostly nano-sized and are otherwise grouped with PP2-NAN (Table 1), this comparison is indicative only. Further details of the data preparation and comparison are provided in Section S.3.4 (Table S33).

Nutrients

Nitrate plus nitrite observations were compiled from Institute of Ocean Sciences bottle data and other sources (Fisheries and Oceans Canada, 2025; Pacific Salmon Foundation (PSF), 2025), standardised to common fields and assigned to the nearest SOGEM-LTL grid cell. Observations were converted to cast-level nutrient inventories over the 0.1–20.0 m layer using trapezoidal integration. Casts were retained when they had at least two sampled depths, the shallowest within 2 m of 0.1 m and the deepest within 2 m of 20.0 m; concentrations at the layer boundaries were then set to the nearest measured value. Cast-level inventories were expressed in areal units (g N m^{-2}).

For model evaluation, dissolved inorganic nitrogen was not available as a direct EwE output and was therefore reconstructed post hoc as a vertically integrated free-nitrogen inventory. In both the Ecosim (non-spatial) and Ecospace (spatial) modules, this was done by closing an areal nitrogen budget in which nitrogen bound in model biomass pools was estimated from modelled biomasses using group-specific C:N multipliers. Free dissolved nitrogen was calculated as the residual required to satisfy the prescribed total nitrogen inventory. This quantity should therefore be interpreted as a diagnostic reconstruction of a generic dissolved nitrogen inventory rather than as a native prognostic tracer simulated by the model.

In the assessment of Ecosim results, observations were matched to the model in time rather than space: cast-level inventories were first reduced to a single value per sampling date, matched to the nearest 3-day Ecosim timestep, and then aggregated to year × biweekly bins prior to climatology construction. In the assessment of Ecospace results, the same observational screening criteria were applied, but model values were extracted from the spatial domain at the corresponding grid cells. Skill was evaluated both using a one-to-one observation versus model output paired table and using a year × biweekly aggregated pairing, allowing comparison between individual cast-level matched pairs and a temporally smoothed representation. Further details of nutrient processing and evaluation are provided in Section S.3.5.

Zooplankton

Zooplankton survey data from the SoG (1996–2018; 2000–2018 used for evaluation, Section S.3.6) were used to evaluate SOGEM-LTL against observed seasonal biomass patterns (Fisheries and Oceans Canada, 2023; Perry et al., 2021). Tow selection, areal integration over each tow's depth range and seasons (winter = December of the preceding year to February) followed Perry et al. (2021) and reproduced their published annual anomalies; survey taxa were assigned to model groups by taxonomy (Section S.3.6). Each tow was matched to the nearest model grid cell and timestep, and the matched tow-level dataset was used for seasonal boxplots and skill statistics.

Because survey effort before 2013 was sparse and irregular (Table S35), interannual variability was evaluated only as annual anomalies of total crustacean biomass for 2015–2018, the only years sampled in every season, calculated identically for observations and tow-matched model output (Perry et al., 2021; Section S.3.6). The relationship between bloom timing and spring crustacean biomass was tested after adjusting tow biomass for sampling date (Section S.3.6).

3. Results

3.1. Spring bloom phenology

SOGEM-LTL Ecospace reproduced interannual variation in satellite-derived bloom timing for 2003–2016 in 13 of 14 years (93%) for the early/average/late bloom category, with good continuous skill (r = 0.77, MAE = 10.5 d, bias = 1.4 d, WSS = 0.86; Table 5, Figure 4). By comparison, the Ecosim configuration showed less agreement with the satellite record, matching 10 of 14 years (71%) and yielding weaker skill statistics (r = 0.65, MAE = 12.9 d, WSS = 0.75). Comparisons of Ecosim and Ecospace outputs against the C09 bloom-timing series showed weaker agreement, with r = 0.36–0.38 and 44–46% of years in the same category (Figure 4; Table 5). For reference, the C09 model itself agreed with the satellite record about as closely as Ecospace (r = 0.77, MAE = 11.1 d, WSS = 0.80; 11 of 14 years correctly categorised; Table 5).

Satellite chlorophyll a and modelled phytoplankton followed a similar seasonal cycle, with a spring maximum in April–May and a smaller autumn increase, but modelled variability was strongly damped (log–log slope 0.08) and week-to-week variation was not reproduced (r = 0.18 after removing the seasonal cycle; Figure 5). The satellite spring increase was concentrated in the central and southern SoG; relative to that pattern, Ecospace was high in the southern passages and low east of the Fraser River plume (within-month spatial r = −0.10 to 0.33; Figure 6).

3.2. Primary productivity and phytoplankton

The annual primary production implied by SOGEM-LTL's balanced Ecopath parameterisation was 374 g C m^{-2} yr^{-1}, within the range of several previous estimates for the SoG (Table S32). At the seasonal scale, phytoplankton biomass and composition were broadly comparable with the reference values for both the Ecosim and Ecospace module outputs (Figure 7). However, the

amplitude of simulated diatom variability was lower than in the reference estimates, indicating that the model captured the broad seasonal pattern more successfully than the full magnitude of variation.

At station QU39, comparison with empirical data showed that SOGEM-LTL reproduced the seasonal pattern of phytoplankton variability, but generally underestimated the spread of observed variability, particularly from spring through fall (Figure 8). Agreement in standardised departures was strongest for dinoflagellates (r = 0.61, WSS = 0.76) and diatoms (r = 0.58, WSS = 0.74), intermediate for picoplankton (r = 0.45, WSS = 0.66), and weakest for nanophytoplankton (r = 0.26, WSS = 0.43; Table S34). The lower modelled intra-month variability relative to the observations further indicates damped simulated variability, especially for nanophytoplankton. This agreement came from the shared seasonal cycle: the model's own monthly climatology matched the observations as closely (r = 0.29–0.62), and departures from that climatology were not correlated (r = −0.16 to 0.27).

3.3. Nutrients

Observed dissolved inorganic nitrogen inventories were strongly seasonal, with clear winter maxima and marked spring-summer depletion (Figure 9). Both model configurations reproduced this in diagnostically reconstructed free-nitrogen inventories, but the Ecosim module more closely tracked the observed seasonal drawdown and recovery than did the Ecospace module. Ecosim achieved moderate skill (n = 68, bias = -0.61 g N m^{-2}, r = 0.64, WSS = 0.70), whereas Ecospace showed lower correspondence (n = 66, bias = 0.58 g N m^{-2}, RMSE = 1.48 g N m^{-2}, r = 0.50, WSS = 0.59). In the climatological comparison, Ecospace tended to maintain excess free nitrogen through much of spring and summer, producing a weaker seasonal drawdown than

observed. An individual cast-level matched Ecospace comparison showed worse agreement (n = 1551, r = 0.29, RMSE = 1.94 g N m^{-2}, WSS = 0.52; Figure S5).

3.4. Zooplankton biomass

SOGEM-LTL Ecospace outputs reproduced the seasonal cycle in zooplankton biomass (Figure 10). For the euphausiid-dominated ZC1-EUP group, both model and observations showed low biomass in winter and spring and higher biomass in summer and fall. Similar agreement was evident for the amphipod-dominated ZC2-AMP group, although summer biomass was underestimated. There was at least one seasonal mismatch per group, with the model tending to underestimate biomass and lag the observed seasonal increase.

Across all crustacean groups and seasons, absolute biomass agreement was modest (r = 0.43, WSS = 0.54; Table S37, Figure S8). Modelled variability was generally lower than observed; for crustacean zooplankton, the standard deviation of log-transformed tow-matched model biomass was approximately half that of the observed tow biomass (Table S37). Results for soft-bodied zooplankton are given in Table S38 and Figures S7 and S9. In both model configurations, years with earlier simulated blooms had higher simulated spring crustacean zooplankton biomass at the surveyed tows after adjusting for sampling date (Ecospace r = −0.61; Ecosim r = −0.77; n = 17 years), and over the full 1980–2018 hindcast (Ecospace r = −0.73; Ecosim r = −0.79; n = 39). Observed spring biomass, adjusted in the same way, was not significantly related to bloom timing (r = −0.23 against C09, n = 17; r = −0.16 against the satellite series, n = 12; Table S39, Figure S10). Observed and modelled annual anomalies of total crustacean biomass for 2015–2018 were positively but not significantly correlated (r = 0.92, p = 0.08, n = 4; Table S36, Figure S6).

4. Discussion

4.1. Physics-forced bloom phenology in EwE

The central result of this study is that interannual variation in spring bloom timing emerged from physical forcing within EwE. Unlike most EwE applications, in which primary production is prescribed or supplied by a biogeochemical model (Section 1), bloom timing in SOGEM-LTL was not prescribed, yet the Ecospace configuration matched the satellite-derived bloom category in 13 of 14 years, with skill comparable to that of the C09 one-dimensional model developed specifically to hindcast bloom timing in the SoG, where timing is controlled mainly by wind-driven mixing and light (Allen and Wolfe, 2013; Collins et al., 2009). The physical controls on the spring transition were therefore carried through EwE's environmental response functions and trophic dynamics at a three-day timestep. To our knowledge, this is the first EwE application in which bloom timing emerges from physical forcing rather than being prescribed.

The approach rests on configuration choices that are transferable to other EwE applications. Rescaling model time so that each model time unit represents one-tenth of a calendar year permits a three-day timestep over multi-decadal simulations within the software's run-length limit. Light- and temperature-response functions applied within Ecosim and Ecospace allow primary production to respond directly to fields from a physical-oceanographic hindcast and an atmospheric reanalysis. An empirical proxy derived from turbulent mixing-layer depth represents vertical nutrient resupply in a model without a vertical dimension, and dissolved inorganic nitrogen can be reconstructed after the run by closing a nitrogen budget. Together, these allow EwE to act as the LTL component of a physics-forced, end-to-end-capable model at a fraction of the computational cost of a three-dimensional biogeochemical model, using a single,

documented workflow (Oldford, 2026a, 2026b). The full 1980–2018 Ecospace hindcast runs in about 35 minutes on a desktop computer (Section 2.3). The evaluation lessons extend beyond EwE: matching the spatial and temporal support of model output and observations, and accounting for sampling dates that vary among years, apply to any process model evaluated against irregular survey or monitoring data (Jakeman et al., 2024).

4.2. Trophic resolution relative to biogeochemical and fisheries applications of EwE

Representation of the zooplankton link is a notable feature of SOGEM-LTL. Zooplankton channel changes in primary production to fish and other upper-trophic-level consumers, yet their functional diversity and seasonal dynamics remain difficult to represent in marine ecosystem models (Eddy et al., 2021; Mackas et al., 2012; Mitra et al., 2014; Ratnarajah et al., 2023). Rather than the one or two zooplankton groups of conventional nutrient–phytoplankton–zooplankton–detritus (NPZD) configurations, SOGEM-LTL resolves three pathways by which production reaches, or bypasses, fish (Section S.2.2). Size structure separates pico-, nano- and diatom-dominated production, and small from large crustacean grazers, with diets constrained by predator–prey size ratios (Hansen et al., 1994). A microbial loop of bacteria, heterotrophic nanoflagellates, ciliates and dinoflagellates recycles dissolved organic carbon and links small phytoplankton to mesozooplankton (Azam et al., 1983; Calbet and Landry, 2004). A gelatinous 'jelly web' of four groups, from scyphozoans to larvaceans, competes with crustaceans for prey and can act either as a trophic dead end or as prey for fish (Hays et al., 2018; Lamb et al., 2019). Seasonal cycles in these groups were not prescribed; they emerged from physical forcing, nutrient constraints and trophic interactions, constrained by the underlying trophic and mortality parameters rather than by fixed seasonal grazing or mortality schedules (Omta et al., 2023; Talmy et al., 2024). Bacteria, heterotrophic nanoflagellates and ciliates could not be evaluated

against local observations, so the microbial pathway remains the least constrained part of the food web.

SOGEM-LTL should be viewed as complementary to, rather than a replacement for, more process-rich regional biogeochemical models. Three-dimensional biogeochemical models remain essential for questions involving oxygen, export production, vertical biogeochemical structure, and fully coupled interactions with ocean circulation (e.g., Holdsworth et al., 2021; Jarníková et al., 2022; Khangaonkar et al., 2012). In the SoG, SOGEM-LTL sits between the one-dimensional C09 model, which hindcasts bloom timing from wind, light and mixing with a minimal food web (Allen and Wolfe, 2013; Collins et al., 2009), and the three-dimensional SalishSeaCast model, which resolves vertical structure and circulation but prescribes mesozooplankton grazing as a seasonal cycle rather than simulating mesozooplankton (Olson et al., 2020; Soontiens et al., 2016; Soontiens and Allen, 2017). Like other models of intermediate complexity, it offers a different set of advantages (Hannah et al., 2010): long hindcasts, relatively rapid scenario exploration, and direct generation of seasonal prey-field indicators.

4.3. Spatial resolution and prey-field dynamics

The spatial Ecospace configuration reproduced bloom timing more closely than the non-spatial Ecosim configuration ($r = 0.77$ versus 0.65; 13 versus 10 of 14 years), although both share the same food web and similar parameter values. One possible reason is that the non-spatial configuration applies nonlinear light, temperature and nutrient responses to domain-averaged forcing, whereas Ecospace applies them locally before biomass is summarised over the domain; resolving spatial variation in mixing and light may therefore improve the timing of the domain-scale spring transition. Because this follows from averaging forcing before applying nonlinear responses, an instance of Jensen's inequality, (Jensen, 1906; Ruel and Ayres, 1999) non-spatial

Ecosim applications driven by area-averaged forcing may misplace the timing of seasonal transitions. Spatial resolution did not improve every indicator: Ecosim reproduced the seasonal nutrient drawdown more closely than Ecospace (Section 3.3), possibly because of the penalty-only environmental responses discussed in Section 4.4. In both model configurations, earlier simulated blooms were followed by higher spring biomass of the crustacean zooplankton that are important prey for Pacific herring and juvenile Pacific salmon, consistent with the match–mismatch mechanisms that motivate the model (Cushing, 1990; Suchy et al., 2022). The survey data did not show this relationship, but with 17 irregularly sampled years and between-year variability in observed spring biomass (yearly means of date-adjusted tows) about three times that simulated, they had little power to detect it. Observed and modelled annual crustacean anomalies were nonetheless positively, but not significantly, correlated for 2015–2018 (Section 3.4). The reconstruction also extends bloom timing and prey fields back to 1980, before the satellite record; these reconstructed conditions are best treated as hypotheses, for example in analyses of Pacific herring recruitment and Pacific salmon survival.

The model reproduced the timing of the spring transition (Table 5, Figure 4) more successfully than later-season dynamics, when it underestimated phytoplankton variability, nitrogen drawdown in Ecospace and summer zooplankton biomass (Figure 8, Figure 9 and Figure 10). A possible explanation for the poorer fit for later-season community succession is that it is affected more strongly by grazing, trophic mediation, vertical fluxes, species turnover, episodic forcing, and nonlinear interactions among phytoplankton, mixotrophs, and metazoan consumers (Sommer et al., 2012; Suchy et al., 2025). These processes were simplified in SOGEM-LTL. Damped variability relative to observations is not unique to SOGEM-LTL: in SalishSeaCast, mesozooplankton grazing follows a prescribed seasonal cycle, so mesozooplankton has no

interannual variability of its own (Olson et al., 2020). It nonetheless remains an important limitation for interpreting the magnitude of events. Modelled phytoplankton variability was similarly damped relative to satellite chlorophyll (Figure 5), partly because near-surface chlorophyll also responds to mixed-layer depth and chlorophyll-to-carbon ratios, which need not change areal biomass.

4.4. Limitations

Evaluation was constrained by sparse and patchy observations. Pairing individual casts or tows with single grid cells and three-day outputs gave poor agreement (dissolved inorganic nitrogen r = 0.29, Figure S5; crustacean zooplankton r = 0.43, Figure S8), whereas monthly to seasonal summaries retained the broad seasonal structure (Figure 8, Figure 9, Figure 10). Because plankton are patchy (Haury et al., 1978; McGillicuddy and Franks, 2019), single samples can differ from grid-cell means even where the model is correct; survey indices estimated at the model's support with spatiotemporal statistical models (Anderson et al., 2025; Gelfand et al., 2001; Thorson et al., 2015) would provide a firmer basis for future evaluation. Where biomass changes rapidly within a season, sampling dates that vary among years also bias season-year means (Jakeman et al., 2024), and zooplankton sampling before 2013 was too sparse and irregular for seasonal interannual comparison (Perry et al., 2021).

Choices concerning spatial and temporal resolution, ecological aggregation, initial conditions, and parameterisation should be distinguished from limitations intrinsic to the EwE framework. The omission of advection removes an ecologically important process in a system where estuarine circulation, lateral transport, and advective seeding may affect both bloom development and zooplankton biomass (e.g., Gower et al., 2013). Ecospace advection was disabled because, with three-day averaged currents, it did not conserve mass and produced

unrealistic biomass oscillations in preliminary tests (Section S.2.8.4). In the present configuration, spatial patterns therefore arise from spatially varying physical forcing acting on local production, trophic interactions and diffusive dispersal among neighbouring cells, rather than from the redistribution of biomass by currents or directed movement; 'spatially resolved' should be read in this sense. Light within the water column was estimated using a proxy PAR sub-model and several influential Ecosim and Ecospace parameters, including predator-prey vulnerability multipliers and movement-related settings, were not exhaustively tuned. The configuration also truncates the wider food web, omitting most upper-trophic-level groups, simplifying or excluding some predation, recycling, detrital, and nutrient-partitioning pathways.

Our study also highlighted limitations intrinsic to the EwE framework. EwE's single generic nutrient currency means the framework cannot directly represent multiple nutrient tracers or coupled biological feedbacks to circulation in the manner of tracer-rich regional biogeochemical or Earth-system models (Christian et al., 2022; Sigmond et al., 2023). The lack of a vertical dimension means that seasonal nutrient resupply had to be approximated empirically, rather than calculated from mechanistic vertical nutrient fluxes. Representing nutrients as inert biomass pools linked to production through mediation may provide another option, but this approach was not tested here. Environmental responses in the current EwE implementation are also effectively penalty-only: they readily suppress realised production under unfavourable conditions but offer less flexibility for representing enhanced rates under particularly favourable conditions. The SOGEM-LTL workaround (Ecosim production multipliers; Table S31) addressed this only partly and differed between Ecosim and Ecospace. This structural limitation may have contributed to the weaker Ecospace nutrient drawdown, but its influence cannot be isolated without targeted sensitivity experiments. Finally, EwE tracks one principal biomass or energy currency at a time,

whereas observations and ecological processes may require conversions that can introduce uncertainty and complicate comparison.

4.5. Extensions

The low computational cost of the present setup makes ensemble-based sensitivity and uncertainty analysis feasible. Global sensitivity and formal parameter-uncertainty analyses were beyond the scope of this study. Parameter ensembles based on Pedigree ranges (Table S14), formal sensitivity analysis, and held-out or cross-validated evaluation would clarify which results are robust. The three-day timestep was also not compared against alternative temporal resolutions, so the sensitivity of bloom timing and seasonal dynamics to this choice is unknown. Ablation experiments in which interannual variability in temperature, irradiance, mixing, or nutrient resupply is removed or replaced with climatologies could identify which physical drivers contribute most strongly to bloom timing and its propagation to zooplankton. Furthermore, the low compute overhead of EwE and convenient stepwise calibration invites automated parameterisation and calibration, an area of rapidly developing methods ranging from metaheuristic parameter search to AI-assisted parameter synthesis (Chou and Molla, 2022; Spillias et al., 2026). Beyond the comparison with satellite chlorophyll, spatial patterns have not been evaluated; spatial surveys, ferry transects or statistically reconstructed fields would be needed before claims are made about spatial gradients, hotspots or local prey conditions.

The reconstruction ends in 2018 because it is forced by the HOTSSea physical hindcast, which covers 1980–2018 (Oldford et al., 2025). More recent physical fields are available from the SalishSeaCast operational system (Olson et al., 2020; Soontiens et al., 2016), but SalishSeaCast begins in 2007 and differs from HOTSSea in horizontal resolution (about 500 m versus 1.5 km), atmospheric forcing and open-boundary conditions (Oldford et al., 2025), so appending it would

introduce a break in the forcing rather than extend a consistent series. Extending SOGEM-LTL beyond 2018 will therefore require either extending HOTSSea or cross-calibrating the two products over the years they overlap. Extension to present would also add several further years of regular zooplankton surveys with which to test the promising 2015–2018 annual agreement.

5. Conclusion

Interannual variation in spring bloom timing emerged from physical forcing in a spatial EwE model without a dedicated biogeochemical model. Positioned between one-dimensional bloom models and three-dimensional biogeochemical models, SOGEM-LTL adds trophic resolution at low computational cost. As an E2E-capable framework, it provides a tractable basis for investigating bottom-up forcing, seasonal match–mismatch, and fisheries-relevant prey dynamics over multi-decadal timescales (Link et al., 2023; Wells and Santora, 2023). Generally, potential applications of the current version concern spring phenology and seasonal prey-field variability, rather than prediction of local biomass, fine-scale community composition or interannual zooplankton anomalies (Cushing, 1990; Ji et al., 2010; Mitra et al., 2014; Suchy et al., 2022). Extending the simulations backward and forward in time becomes increasingly feasible using the EwE-based approach documented here, and doing so would support investigation of Pacific herring recruitment anomalies, Pacific salmon survival shifts, and ecosystem responses to regional climate regimes (Boldt et al., 2025; Hare and Mantua, 2000). In this role, SOGEM-LTL contributes to broader efforts to develop integrated, regionally relevant ecosystem reconstructions for marine research and management.

CRediT authorship contribution statement

Greig Oldford: Conceptualization, Methodology, Software, Formal analysis, Investigation, Data curation, Validation, Visualization, Resources, Funding acquisition, Project administration, Writing – original draft, Writing – review & editing.

Brian Hunt: Conceptualization, Supervision, Visualization, Writing – review & editing.

Carl Walters: Conceptualization, Methodology, Supervision, Writing – review & editing.

Villy Christensen: Conceptualization, Methodology, Software, Formal analysis, Resources, Supervision, Funding acquisition, Writing – review & editing.

Acknowledgements: The authors wish to thank Isobel Pearsall, Joe Buszowski, Jeroen Steenbeek, Marta Coll, and members of the Ecopath International Initiative for their advice and feedback. The authors also acknowledge the support of Eddy Kennedy, Carmel Lowe, Brigid Payne, Brian Riddell, the Pacific Salmon Foundation, and the Department of Fisheries and Oceans, Canada. The authors benefited from the feedback and guidance provided by Akash Sastri, Ian Perry, Chrys Neville, Jennifer Boldt, Kelly Young, Moira Galbraith, Susan Allen, Elise Olson, Michael Dunphy, Anna McLaskey, Karyn Suchy, Rich Pawlowicz, Richard Beamish, Florian Lüskow, Colette Wabnitz, Hem Morzaria Luna, and Isaac Kaplan. We thank Maycira Costa (University of Victoria) for providing the satellite chlorophyll a data.

Financial support. This research has been supported by the Mitacs Accelerate programme (grant no. IT12313), Fisheries and Oceans Canada (Government of Canada), the Pacific Salmon Foundation, the University of British Columbia (UBC), the UBC Ocean Leaders programme, and the Salish Sea Marine Survival Project.

Declaration of generative AI and AI-assisted technologies in the manuscript preparation process: During the preparation of this work, the author(s) used OpenAI tools (ChatGPT) to support development of code used in model evaluation and Anthropic tools (Claude) for

revisions of code used for evaluation, checking grammar and suggesting changes of the manuscript, finding and fixing errors in the reference list, and organizing the Supplement. The author(s) reviewed and edited the output as needed and take full responsibility for the content of the published article.

673

References

674 675 676 677 Aalderink, R.H., Jovin, R., 1997. Estimation of the photosynthesis/irradiance (P/I) curve parameters from light and dark bottle experiments. J. Plankton Res. 19, 1713–1742. https://doi.org/10.1093/plankt/19.11.1713

678 679 680 681 Akoglu, E., Libralato, S., Salihoglu, B., Oguz, T., Solidoro, C., 2015. EwE-F 1.0: an implementation of Ecopath with Ecosim in Fortran 95/2003 for coupling and integration with other models. Geosci. Model Dev. 8, 2687–2699. https://doi.org/10.5194/gmd-8-2687-2015

682 683 684 Allen, S.E., Wolfe, M.A., 2013. Hindcast of the timing of the spring phytoplankton bloom in the Strait of Georgia, 1968-2010. Prog. Oceanogr. 115, 6–13. https://doi.org/10.1016/j.pocean.2013.05.026

685 686 687 688 Anderson, S.C., Ward, E.J., English, P.A., Barnett, L.A.K., Thorson, J.T., 2025. sdmTMB: An R Package for Fast, Flexible, and User-Friendly Generalized Linear Mixed Effects Models with Spatial and Spatiotemporal Random Fields. J. Stat. Softw. 115, 1–46. https://doi.org/10.18637/jss.v115.i02

689 690 691 Anderson, S.I., Barton, A.D., Clayton, S., Dutkiewicz, S., Rynearson, T.A., 2021. Marine phytoplankton functional types exhibit diverse responses to thermal change. Nat. Commun. 12, 6413. https://doi.org/10.1038/s41467-021-26651-8

692 693 694 695 Araignous, E., Bourdaud, P., Le Marchand, M., Marzloff, M.P., Ben Rais Lasram, F., Niquil, N., Halouani, G., Safi, G., Le Loc'h, F., 2026. An end-to-end modelling approach to evaluate different facets of climate change on the Eastern channel and southern North Sea ecosystem. J. Mar. Syst. 258, 104279. https://doi.org/10.1016/j.jmarsys.2026.104279

696 697 698 Azam, F., Fenchel, T., Field, J.G., Gray, J.S., Meyer-Reil, L.A., Thingstad, F., 1983. The Ecological Role of Water-Column Microbes in the Sea. Mar. Ecol. Prog. Ser. 10, 257–263.

699 700 701 Beamish, R.J., Noakes, D.J., McFarlane, G.A., Klyashtorin, L., Ivanov, V.V., Kurashov, V., 1999. The regime concept and natural trends in the production of Pacific salmon. Can. J. Fish. Aquat. Sci. 56, 516–526. https://doi.org/10.1139/f98-200

702 703 704 Beamish, R.J., Sweeting, R.M., Neville, C.M., 2004. Improvement of Juvenile Pacific Salmon Production in a Regional Ecosystem after the 1998 Climatic Regime Shift. Trans. Am. Fish. Soc. 133, 1163–1175. https://doi.org/10.1577/t03-170.1

705 706 707 Behrenfeld, M.J., Boss, E.S., 2014. Resurrecting the ecological underpinnings of ocean plankton blooms. Annu. Rev. Mar. Sci. 6, 167–194. https://doi.org/10.1146/annurev-marine-052913-021325

708 709 710 711 Boldt, J.L., Rooper, C.N., Cleary, J.S., Fu, C., Edwards, A.M., Hourston, R.A.S., Peña, M.A., Perry, R.I., 2025. Incorporating ecosystem information into science advice for fisheries management—a case study for Haida Gwaii Pacific herring. Can. J. Fish. Aquat. Sci. 82, 1–26. https://doi.org/10.1139/cjfas-2024-0150

712 713 714 Calbet, A., Landry, M.R., 2004. Phytoplankton growth, microzooplankton grazing, and carbon cycling in marine systems. Limnol. Oceanogr. 49, 51–57. https://doi.org/10.4319/lo.2004.49.1.0051

715 Chenillat, F., Rivière, P., Ohman, M.D., 2021. On the sensitivity of plankton ecosystem models
716 to the formulation of zooplankton grazing. PLOS ONE 16, e0252033.
717 https://doi.org/10.1371/journal.pone.0252033
718 Chou, J.-S., Molla, A., 2022. Recent advances in use of bio-inspired jellyfish search algorithm
719 for solving optimization problems. Sci. Rep. 12, 19157. https://doi.org/10.1038/s41598-
720 022-23121-z
721 Christensen, V., Coll, M., Steenbeek, J., Buszowski, J., Chagaris, D., Walters, C.J., 2014.
722 Representing Variable Habitat Quality in a Spatial Food Web Model. Ecosystems 17,
723 1397–1412. https://doi.org/10.1007/s10021-014-9803-3
724 Christensen, V., Steenbeek, J., 2024. User Guide for Ecopath with Ecosim (EwE). The
725 University of British Columbia.
726 Christensen, V., Walters, C.J., 2024. Ecosystem Modelling with EwE. The University of British
727 Columbia, Vancouver, BC. https://doi.org/10.14288/24d7-ab68
728 Christensen, V., Walters, C.J., 2005. Ecopath with Ecosim: A User's Guide. Fisheries Centre,
729 University of British Columbia, Vancouver.
730 Christian, J.R., Denman, K.L., Hayashida, H., Holdsworth, A.M., Lee, W.G., Riche, O.G.J.,
731 Shao, A.E., Steiner, N., Swart, N.C., 2022. Ocean biogeochemistry in the Canadian Earth
732 System Model version 5.0.3: CanESM5 and CanESM5-CanOE. Geosci. Model Dev. 15,
733 4393–4424. https://doi.org/10.5194/gmd-15-4393-2022
734 Coll, M., Steenbeek, J., Pennino, M.G., Buszowski, J., Fortibuoni, T., Link, J., Kearney, K.,
735 Kaschner, K., Lotze, H.K., Rousseau, Y., Tittensor, D.P., Walters, C., Watson, R.A.,
736 Christensen, V., 2020. Advancing Global Ecological Modeling Capabilities to Simulate
737 Future Trajectories of Change in Marine Ecosystems. Front. Mar. Sci. 7, 567877.
738 https://doi.org/10.3389/fmars.2020.567877
739 Colléter, M., Valls, A., Guitton, J., Gascuel, D., Pauly, D., Christensen, V., 2015. Global
740 overview of the applications of the Ecopath with Ecosim modeling approach using the
741 EcoBase models repository. Ecol. Model. 302, 42–53.
742 https://doi.org/10.1016/j.ecolmodel.2015.01.025
743 Collins, A.K., Allen, S.E., Pawlowicz, R., 2009. The role of wind in determining the timing of
744 the spring bloom in the Strait of Georgia. Can. J. Fish. Aquat. Sci. 66, 1597–1616.
745 https://doi.org/10.1139/F09-071
746 Coronado, C., Hilborn, R., 1998. Spatial and Temporal Factors Affecting Survival in Coho and
747 Fall Chinook Salmon in the Pacific Northwest. Bull. Mar. Sci. 62, 409–425.
748 Crowley, P.H., 1975. Natural selection and the Michaelis constant. J. Theor. Biol. 50, 461–475.
749 https://doi.org/10.1016/0022-5193(75)90093-4
750 Cushing, D.H., 1990. Plankton production and year-class strength in fish populations: an update
751 of the match/mismatch hypothesis, in: Advances in Marine Biology. Academic Press, pp.
752 249–293. https://doi.org/10.1016/S0065-2881(08)60202-3
753 Cushing, D.H., 1971. Upwelling and the Production of Fish, in: Russell, F.S., Yonge, M. (Eds.),
754 Advances in Marine Biology. Academic Press, pp. 255–334.
755 https://doi.org/10.1016/S0065-2881(08)60344-2
756 de Mutsert, K., Coll, M., Steenbeek, J., Ainsworth, C., Buszowski, J., Chagaris, D., Christensen,
757 V., Heymans, S.J.J., Lewis, K.A., Libralato, S., Oldford, G., Piroddi, C., Romagnoni, G.,
758 Serpetti, N., Spence, M.A., Walters, C., 2023. Advances in spatial-temporal coastal and
759 marine ecosystem modeling using Ecospace., in: Reference Module in Earth Systems and
760 Environmental Sciences. Elsevier. https://doi.org/10.1016/B978-0-323-90798-9.00035-4

de Mutsert, K., Steenbeek, J., Lewis, K., Buszowski, J., Cowan, J.H., Christensen, V., 2016. Exploring effects of hypoxia on fish and fisheries in the northern Gulf of Mexico using a dynamic spatially explicit ecosystem model. Ecol. Model. 331, 142–150. https://doi.org/10.1016/j.ecolmodel.2015.10.013

Del Bel Belluz, J., 2024. Protistan plankton time series from the northern Salish Sea and central coast, British Columbia, Canada - Ocean Biodiversity Information System.

Del Bel Belluz, J., Peña, M.A., Jackson, J.M., Nemcek, N., 2021. Phytoplankton Composition and Environmental Drivers in the Northern Strait of Georgia (Salish Sea), British Columbia, Canada. Estuaries Coasts 44, 1419–1439. https://doi.org/10.1007/s12237-020-00858-2

Dişa, D., Akoglu, E., Salihoglu, B., 2024. Exploitation of mesopelagic fish stocks can impair the biological pump and food web dynamics in the ocean. Front. Mar. Sci. 11, 1389941. https://doi.org/10.3389/fmars.2024.1389941

Eddy, T.D., Bernhardt, J.R., Blanchard, J.L., Cheung, W.W.L., Colléter, M., du Pontavice, H., Fulton, E.A., Gascuel, D., Kearney, K.A., Petrik, C.M., Roy, T., Rykaczewski, R.R., Selden, R., Stock, C.A., Wabnitz, C.C.C., Watson, R.A., 2021. Energy Flow Through Marine Ecosystems: Confronting Transfer Efficiency. Trends Ecol. Evol. 36, 76–86. https://doi.org/10.1016/j.tree.2020.09.006

Fisheries and Oceans Canada, 2025. Seawater properties measured from Niskin bottle samples collected in British Columbia, Canada, 1930 to present - CIOOS/SIOOC.

Fisheries and Oceans Canada, 2023. Zooplankton data from central and northern Strait of Georgia - Open Government Portal [WWW Document]. URL https://open.canada.ca/data/en/dataset/2822c11d-6b6c-437e-ad65-85f584522adc (accessed 3.8.24).

Franks, P.J.S., 2015. Has Sverdrup's critical depth hypothesis been tested? Mixed layers vs. turbulent layers. ICES J. Mar. Sci. 72, 1897–1907. https://doi.org/10.1093/icesjms/fsu175

Friedland, K.D., Stock, C., Drinkwater, K.F., Link, J.S., Leaf, R.T., Shank, B.V., Rose, J.M., Pilskaln, C.H., Fogarty, M.J., 2012. Pathways between Primary Production and Fisheries Yields of Large Marine Ecosystems. PLOS ONE 7, e28945. https://doi.org/10.1371/journal.pone.0028945

Fulton, E.A., Blanchard, J.L., Melbourne-Thomas, J., Plagányi, É.E., Tulloch, J.D.V., 2019. Where the Ecological Gaps Remain, a Modelers' Perspective. Front. Ecol. Evol. 7, 424. https://doi.org/10.3389/fevo.2019.00424

Gargett, A.E., 1997. Physics to fish: Interactions between physics and biology on a variety of scales. Oceanography 10, 128–131. https://doi.org/10.5670/oceanog.1997.05

Gasset, N., Fortin, V., Dimitrijevic, M., Carrera, M., Bilodeau, B., Muncaster, R., Gaborit, É., Roy, G., Pentcheva, N., Bulat, M., Wang, X., Pavlovic, R., Lespinas, F., Khedhaouiria, D., Mai, J., 2021. A 10 km North American precipitation and land-surface reanalysis based on the GEM atmospheric model. Hydrol. Earth Syst. Sci. 25, 4917–4945. https://doi.org/10.5194/hess-25-4917-2021

Gelfand, A.E., Zhu, L., Carlin, B.P., 2001. On the change of support problem for spatio-temporal data. Biostatistics 2, 31–45. https://doi.org/10.1093/biostatistics/2.1.31

Gower, J., King, S., Statham, S., Fox, R., Young, E., 2013. The Malaspina Dragon: A newly-discovered pattern of the early spring bloom in the Strait of Georgia, British Columbia, Canada. Prog. Oceanogr. 115, 181–188. https://doi.org/10.1016/j.pocean.2013.05.024

Hannah, C., Vezina, A., St. John, M., 2010. The case for marine ecosystem models of intermediate complexity. Prog. Oceanogr. 84, 121–128. https://doi.org/10.1016/j.pocean.2009.09.015

Hansen, B., Bjornsen, P.K., Hansen, P.J., 1994. The size ratio between planktonic predators and their prey. Limnol. Oceanogr. 39, 395–403. https://doi.org/10.4319/lo.1994.39.2.0395

Hare, S.R., Mantua, N.J., 2000. Empirical evidence for North Pacific regime shifts in 1977 and 1989. Prog. Oceanogr. 47, 103–145. https://doi.org/10.1016/S0079-6611(00)00033-1

Harrison, P.J., Fulton, J.D., Taylor, F.J.R., Parsons, T.R., 1983. Review of the Biological Oceanography of the Strait of Georgia: Pelagic Environment. Can. J. Fish. Aquat. Sci. 40, 1064–1094. https://doi.org/10.1139/f83-129

Haury, L.R., McGowan, J.A., Wiebe, P.H., 1978. Patterns and Processes in the Time-Space Scales of Plankton Distributions, in: Steele, J.H. (Ed.), Spatial Pattern in Plankton Communities. Springer US, Boston, MA, pp. 277–327. https://doi.org/10.1007/978-1-4899-2195-6_12

Hays, G.C., Doyle, T.K., Houghton, J.D.R., 2018. A Paradigm Shift in the Trophic Importance of Jellyfish? Trends Ecol. Evol. 33, 874–884. https://doi.org/10.1016/J.TREE.2018.09.001

Heneghan, R.F., Galbraith, E., Blanchard, J.L., Harrison, C., Barrier, N., Bulman, C., Cheung, W., Coll, M., Eddy, T.D., Erauskin-Extramiana, M., Everett, J.D., Fernandes-Salvador, J.A., Gascuel, D., Guiet, J., Maury, O., Palacios-Abrantes, J., Petrik, C.M., du Pontavice, H., Richardson, A.J., Steenbeek, J., Tai, T.C., Volkholz, J., Woodworth-Jefcoats, P.A., Tittensor, D.P., 2021. Disentangling diverse responses to climate change among global marine ecosystem models. Prog. Oceanogr. 198, 102659. https://doi.org/10.1016/j.pocean.2021.102659

Heymans, J.J., Coll, M., Link, J.S., Mackinson, S., Steenbeek, J., Walters, C., Christensen, V., 2016. Best practice in Ecopath with Ecosim food-web models for ecosystem-based management. Ecol. Model. 331, 173–184. https://doi.org/10.1016/j.ecolmodel.2015.12.007

Holdsworth, A.M., Zhai, L., Lu, Y., Christian, J.R., 2021. Future Changes in Oceanography and Biogeochemistry Along the Canadian Pacific Continental Margin. Front. Mar. Sci. 8, 602991. https://doi.org/10.3389/fmars.2021.602991

Huisman, J., Sharples, J., Stroom, J.M., Visser, P.M., Kardinaal, W.E.A., Verspagen, J.M.H., Sommeijer, B., 2004. Changes in Turbulent Mixing Shift Competition for Light Between Phytoplankton Species. Ecology 85, 2960–2970. https://doi.org/10.1890/03-0763

Huisman, J., Van Oostveen, P., Weissing, F.J., 1999. Critical depth and critical turbulence: Two different mechanisms for the development of phytoplankton blooms. Limnol. Oceanogr. 44, 1781–1787. https://doi.org/10.4319/lo.1999.44.7.1781

Jakeman, A.J., Elsawah, S., Wang, H.-H., Hamilton, S.H., Melsen, L., Grimm, V., 2024. Towards normalizing good practice across the whole modeling cycle: its instrumentation and future research topics. Socio-Environ. Syst. Model. 6, 18755. https://doi.org/10.18174/sesmo.18755

Jarníková, T., Ianson, D., Allen, S.E., Shao, A.E., Olson, E.M., 2022. Anthropogenic Carbon Increase has Caused Critical Shifts in Aragonite Saturation Across a Sensitive Coastal System. Glob. Biogeochem. Cycles 36, e2021GB007024. https://doi.org/10.1029/2021GB007024

Jassby, A.D., Platt, T., 1976. Mathematical formulation of the relationship between photosynthesis and light for phytoplankton. Limnol. Oceanogr. 21, 540–547. https://doi.org/10.4319/lo.1976.21.4.0540
Jensen, J.L., 1906. Sur les fonctions convexes et les inégalités entre les valeurs moyennes. Acta Mathematica 30, 175-193.
Ji, R., Edwards, M., Mackas, D.L., Runge, J.A., Thomas, A.C., 2010. Marine plankton phenology and life history in a changing climate: current research and future directions. J. Plankton Res. 32, 1355–1368. https://doi.org/10.1093/plankt/fbq062
Johannessen, S.C., Macdonald, R.W., 2009. Effects of local and global change on an inland sea: the Strait of Georgia, British Columbia, Canada. Clim. Res. 40, 1–21. https://doi.org/10.3354/cr00819
Johannessen, S.C., Macdonald, R.W., Paton, D.W., 2003. A sediment and organic carbon budget for the greater Strait of Georgia. Estuar. Coast. Shelf Sci. 56, 845–860. https://doi.org/10.1016/S0272-7714(02)00303-7
Kaschner, K., Kesner-Reyes, K., Garilao, C., Segschneider, J., Rius-Barile, J., Rees, T., Froese, R., 2023. AquaMaps: Predicted range maps for aquatic species [WWW Document]. AquaMaps. URL https://www.aquamaps.org
Kearney, K.A., Bograd, S.J., Drenkard, E., Gomez, F.A., Haltuch, M., Hermann, A.J., Jacox, M.G., Kaplan, I.C., Koenigstein, S., Luo, J.Y., Masi, M., Muhling, B., Pozo Buil, M., Woodworth-Jefcoats, P.A., 2021. Using Global-Scale Earth System Models for Regional Fisheries Applications. Front. Mar. Sci. 8, 622206. https://doi.org/10.3389/fmars.2021.622206
Khangaonkar, T., Nugraha, A., Yun, S.K., Premathilake, L., Keister, J.E., Bos, J., 2021. Propagation of the 2014–2016 Northeast Pacific Marine Heatwave Through the Salish Sea. Front. Mar. Sci. 8, 787604. https://doi.org/10.3389/fmars.2021.787604
Khangaonkar, T., Sackmann, B., Long, W., Mohamedali, T., Roberts, M., 2012. Simulation of annual biogeochemical cycles of nutrient balance, phytoplankton bloom(s), and DO in Puget Sound using an unstructured grid model. Ocean Dyn. 62, 1353–1379. https://doi.org/10.1007/s10236-012-0562-4
Kiørboe, T., 2018. A Mechanistic Approach to Plankton Ecology. Princeton University Press. https://doi.org/10.1515/9780691190310
Lamb, P.D., Hunter, E., Pinnegar, J.K., Doyle, T.K., Creer, S., Taylor, M.I., Coll, M., 2019. Inclusion of jellyfish in 30+ years of Ecopath with Ecosim models. ICES J. Mar. Sci. 76, 1941–1950. https://doi.org/10.1093/ICESJMS/FSZ165
Li, M., Gargett, A., Denman, K., 2000. What determines seasonal and interannual variability of phytoplankton and zooplankton in strongly estuarine systems? Application to the semi-enclosed estuary of Strait of Georgia and Juan de Fuca Strait. Estuar. Coast. Shelf Sci. 50, 467–488. https://doi.org/10.1006/ecss.2000.0593
Libralato, S., Solidoro, C., 2009. Bridging biogeochemical and food web models for an End-to-End representation of marine ecosystem dynamics: The Venice lagoon case study. Ecol. Model. 220, 2960–2971. https://doi.org/10.1016/j.ecolmodel.2009.08.017
Link, J.S., 2010. Adding rigor to ecological network models by evaluating a set of pre-balance diagnostics: A plea for PREBAL. Ecol. Model. 221, 1580–1591. https://doi.org/10.1016/j.ecolmodel.2010.03.012

Link, J.S., Thur, S., Matlock, G., Grasso, M., 2023. Why we need weather forecast analogues for marine ecosystems. ICES J. Mar. Sci. 80, 2087–2098. https://doi.org/10.1093/icesjms/fsad143

Mackas, D.L., Greve, W., Edwards, M., Chiba, S., Tadokoro, K., Eloire, D., Mazzocchi, M.G., Batten, S., Richardson, A.J., Johnson, C., Head, E., Conversi, A., Peluso, T., 2012. Changing zooplankton seasonality in a changing ocean: Comparing time series of zooplankton phenology. Prog. Oceanogr. 97–100, 31–62. https://doi.org/10.1016/j.pocean.2011.11.005

Mackas, D.L., Harrison, P.J., 1997. Nitrogenous nutrient sources and sinks in the Juan de Fuca Strait/Strait of Georgia/Puget Sound estuarine system: Assessing the potential for eutrophication. Estuar. Coast. Shelf Sci. 44, 1–21. https://doi.org/10.1006/ecss.1996.0110

Martin, A.P., Dominguez, A.B., Baker, C.A., Baumas, C.M.J., Bisson, K.M., Cavan, E., Freilich, M., Galbraith, E., Galí, M., Henson, S., Kvale, K.F., Lemmen, C., Luo, J.Y., McMonagle, H., Viríssimo, F. de M., Möller, K.O., Richon, C., Suresh, I., Wilson, J.D., Woodstock, M.S., Yool, A., 2024. When to add a new process to a model – and when not: A marine biogeochemical perspective. Ecol. Model. 498, 110870. https://doi.org/10.1016/j.ecolmodel.2024.110870

McEwan, N., Pawlowicz, R., Pakhomov, E., Maldonado, M.T., 2023. Seasonality of modelled planktonic food web structure in the Strait of Georgia, Canada. Ecol. Model. 482, 110402. https://doi.org/10.1016/j.ecolmodel.2023.110402

McGillicuddy, D.J., Franks, P.J.S., 2019. Models of plankton patchiness, in: Encyclopedia of Ocean Sciences. Academic Press, Cambridge, MA, pp. 536–546.

Mitra, A., Castellani, C., Gentleman, W.C., Jónasdóttir, S.H., Flynn, K.J., Bode, A., Halsband, C., Kuhn, P., Licandro, P., Agersted, M.D., Calbet, A., Lindeque, P.K., Koppelmann, R., Møller, E.F., Gislason, A., Nielsen, T.G., St. John, M., 2014. Bridging the gap between marine biogeochemical and fisheries sciences; configuring the zooplankton link. Prog. Oceanogr. 129, 176–199. https://doi.org/10.1016/j.pocean.2014.04.025

Morales-Zárate, M.V., Stavrinaky-Suarez, A., Zamora-García, O., Quimbar, J., 2026. Ecosystem-based modeling of Pacific hake (*Merluccius productus*) in the Gulf of California: Evidence of potential functional redundancy and fisheries implications. Ecol. Model. 522, 111802. https://doi.org/10.1016/j.ecolmodel.2026.111802

Oka, K., Sohma, A., 2026. Trophic modeling of temperature, nutrient, and hypoxia dynamics on Japanese anchovy populations in Osaka Bay. Ecol. Model. 514, 111467. https://doi.org/10.1016/j.ecolmodel.2025.111467

Oldford, G., 2026a. SOGEM-LTL data. https://doi.org/10.5281/zenodo.20301932

Oldford, G., 2026b. SOGEM-LTL-code. https://doi.org/10.5281/zenodo.20350052

Oldford, G., Jarníková, T., Christensen, V., Dunphy, M., 2025. HOTSSea v1: a NEMO-based physical Hindcast of the Salish Sea (1980-2018) supporting ecosystem model development. Geosci. Model Dev. 18, 211–237. https://doi.org/10.5194/gmd-18-211-2025

Olson, E.M., Allen, S.E., Do, V., Dunphy, M., Ianson, D., 2020. Assessment of Nutrient Supply by a Tidal Jet in the Northern Strait of Georgia Based on a Biogeochemical Model. J. Geophys. Res. Oceans 125, e2019JC015766. https://doi.org/10.1029/2019JC015766

Omta, A.W., Heiny, E.A., Rajakaruna, H., Talmy, D., Follows, M.J., 2023. Trophic model closure influences ecosystem response to enrichment. Ecol. Model. 475, 110183. https://doi.org/10.1016/j.ecolmodel.2022.110183

Pacific Salmon Foundation (PSF), 2025. Citizen Science Oceanography Program.
Pearsall, I., Schmidt, M., Kemp, I., Riddell, B., 2021. Factors Limiting Survival of Juvenile Chinook Salmon, Coho Salmon and Steelhead in the Salish Sea: Synthesis of Findings of the Salish Sea Marine Survival Project (No. 1), Salish Sea Marine Survival Project. Pacific Salmon Foundation, Vancouver, BC.
Perry, R.I., Galbraith, M., Young, K., Chandler, P., Velez-Espino, A., Baillie, S., 2021. Zooplankton variability in the Strait of Georgia, Canada, and relationships with the marine survivals of Chinook and Coho salmon. PLoS ONE 16, e0245941. https://doi.org/10.1371/journal.pone.0245941
Perry, R.I., Masson, D., 2013. An integrated analysis of the marine social-ecological system of the Strait of Georgia, Canada, over the past four decades, and development of a regime shift index. Prog. Oceanogr. 115, 14–27. https://doi.org/10.1016/j.pocean.2013.05.021
Petrik, C.M., Luo, J.Y., Heneghan, R.F., Everett, J.D., Harrison, C.S., Richardson, A.J., 2022. Assessment and Constraint of Mesozooplankton in CMIP6 Earth System Models. Glob. Biogeochem. Cycles 36, e2022GB007367. https://doi.org/10.1029/2022GB007367
Ratnarajah, L., Abu-Alhaija, R., Atkinson, A., Batten, S., Bax, N.J., Bernard, K.S., Canonico, G., Cornils, A., Everett, J.D., Grigoratou, M., Ishak, N.H.A., Johns, D., Lombard, F., Muxagata, E., Ostle, C., Pitois, S., Richardson, A.J., Schmidt, K., Stemmann, L., Swadling, K.M., Yang, G., Yebra, L., 2023. Monitoring and modelling marine zooplankton in a changing climate. Nat. Commun. 14, 564. https://doi.org/10.1038/s41467-023-36241-5
Riche, O., Johannessen, S.C., Macdonald, R.W., 2014. Why timing matters in a coastal sea: Trends, variability and tipping points in the Strait of Georgia, Canada. J. Mar. Syst. 131, 36–53. https://doi.org/10.1016/j.jmarsys.2013.11.003
Rose, K.A., Allen, J.I., Artioli, Y., Barange, M., Blackford, J., Carlotti, F., Creekmore, S., Cropp, R., Daewel, U., Edwards, K., Flynn, K., Hill, S.L., HilleRisLambers, R., Huse, G., Mackinson, S., Mergrey, B., Moll, A., Rivkin, R., Salihoglu, B., Schrum, C., Shannon, L., Shin, Y., Smith, S.L., Smith, C., Solidoro, C., St. John, M., Zhou, M., 2010. End-To-End Models for the Analysis of Marine Ecosystems: Challenges, Issues, and Next Steps. Mar. Coast. Fish. Dyn. Manag. Ecosyst. Sci. 2, 115–130. https://doi.org/10.1577/C09-059.1
Ruel, J.J., Ayres, M.P., 1999. Jensen's inequality predicts effects of environmental variation. Trends Ecol. Evol. 14, 361–366.
Ruff, C.P., Anderson, J.H., Kemp, I.M., Kendall, N.W., McHugh, P.A., Velez-Espino, A., Greene, C.M., Trudel, M., Holt, C.A., Ryding, K.E., Rawson, K., 2017. Salish Sea Chinook salmon exhibit weaker coherence in early marine survival trends than coastal populations. Fish. Oceanogr. 26, 625–637. https://doi.org/10.1111/fog.12222
Sarmiento, J.L., Gruber, N., 2006. Ocean biogeochemical dynamics. Princeton University Press, Princeton. https://doi.org/10.1515/9781400849079
Sigmond, M., Anstey, J., Arora, V., Digby, R., Gillett, N., Kharin, V., Merryfield, W., Reader, C., Scinocca, J., Swart, N., Virgin, J., Abraham, C., Cole, J., Lambert, N., Lee, W.-S., Liang, Y., Malinina, E., Rieger, L., von Salzen, K., Seiler, C., Seinen, C., Shao, A., Sospedra-Alfonso, R., Wang, L., Yang, D., 2023. Improvements in the Canadian Earth System Model (CanESM) through systematic model analysis: CanESM5.0 and CanESM5.1. Geosci. Model Dev. 16, 6553–6591. https://doi.org/10.5194/gmd-16-6553-2023

Sobocinski, K.L., Greene, C.M., Anderson, J.H., Kendall, N.W., Schmidt, M.W., Zimmerman, M.S., Kemp, I.M., Kim, S., Ruff, C.P., 2021. A hypothesis-driven statistical approach for identifying ecosystem indicators of coho and Chinook salmon marine survival. Ecol. Indic. 124, 107403. https://doi.org/10.1016/j.ecolind.2021.107403

Sommer, U., Adrian, R., Domis, L.D.S., Elser, J.J., Gaedke, U., Ibelings, B., Jeppesen, E., Lürling, M., Molinero, J.C., Mooij, W.M., Donk, E. van, Winder, M., 2012. Beyond the Plankton Ecology Group (PEG) Model: Mechanisms Driving Plankton Succession. Annu. Rev. Ecol. Evol. Syst. 43, 429–448. https://doi.org/10.1146/annurev-ecolsys-110411-160251

Soontiens, N., Allen, S.E., 2017. Modelling sensitivities to mixing and advection in a sill-basin estuarine system. Ocean Model. 112, 17–32. https://doi.org/10.1016/j.ocemod.2017.02.008

Soontiens, N., Allen, S.E., Latornell, D., Le Souëf, K., Machuca, I., Paquin, J.-P., Lu, Y., Thompson, K., Korabel, V., 2016. Storm Surges in the Strait of Georgia Simulated with a Regional Model. Atmos.-Ocean 54, 1–21. https://doi.org/10.1080/07055900.2015.1108899

Spillias, S., Fulton, E.A., Boschetti, F., Bulman, C., Strzelecki, J., Trebilco, R., 2026. AI-driven knowledge synthesis for food web parameterisation. Environ. Model. Softw. 197, 106865. https://doi.org/10.1016/j.envsoft.2026.106865

Steenbeek, J., Buszowski, J., Chagaris, D., Christensen, V., Coll, M., Fulton, E.A., Katsanevakis, S., Lewis, K.A., Mazaris, A.D., Macias, D., de Mutsert, K., Oldford, G., Pennino, M.G., Piroddi, C., Romagnoni, G., Serpetti, N., Shin, Y.-J., Spence, M.A., Stelzenmüller, V., 2021. Making spatial-temporal marine ecosystem modelling better – A perspective. Environ. Model. Softw. 145, 105209. https://doi.org/10.1016/j.envsoft.2021.105209

Steenbeek, J., Coll, M., Gurney, L., Mélin, F., Hoepffner, N., Buszowski, J., Christensen, V., 2013. Bridging the gap between ecosystem modeling tools and geographic information systems: Driving a food web model with external spatial-temporal data. Ecol. Model. 263, 139–151. https://doi.org/10.1016/j.ecolmodel.2013.04.027

Stenseth, N.C., Mysterud, A., Ottersen, G., Hurrell, J.W., Chan, K.-S., Lima, M., 2002. Ecological Effects of Climate Fluctuations. Science 297, 1292–1296. https://doi.org/10.1126/science.1071281

Stock, C.A., John, J.G., Rykaczewski, R.R., Asch, R.G., Cheung, W.W.L., Dunne, J.P., Friedland, K.D., Lam, V.W.Y., Sarmiento, J.L., Watson, R.A., 2017. Reconciling fisheries catch and ocean productivity. Proc. Natl. Acad. Sci. U. S. A. 114, E1441–E1449. https://doi.org/10.1073/pnas.1610238114

Suchy, K.D., Allen, S.E., Olson, E., 2025. Mechanistic Links Between Climatic Forcing and Model-Based Plankton Dynamics in the Strait of Georgia, Canada. J. Geophys. Res. Oceans 130, e2024JC021036. https://doi.org/10.1029/2024JC021036

Suchy, K.D., Young, K., Galbraith, M., Perry, R.I., Costa, M., 2022. Match/Mismatch Between Phytoplankton and Crustacean Zooplankton Phenology in the Strait of Georgia, Canada. Front. Mar. Sci. 9, 832684. https://doi.org/10.3389/fmars.2022.832684

Susini, I., Todd, V.L.G., 2021. Predictive capacity of Ecopath with Ecosim: Model performance and ecological indicators' response to imprecision. Environ. Model. Softw. 143, 105098. https://doi.org/10.1016/J.ENVSOFT.2021.105098

Sutton, J.N., Johannessen, S.C., Macdonald, R.W., 2013. A nitrogen budget for the Strait of Georgia, British Columbia, with emphasis on particulate nitrogen and dissolved inorganic nitrogen. Biogeosciences 10, 7179–7194. https://doi.org/10.5194/bg-10-7179-2013

Talmy, D., Carr, E., Rajakaruna, H., Våge, S., Omta, A.W., 2024. Killing the predator: impacts of highest-predator mortality on the global-ocean ecosystem structure. Biogeosciences 21, 2493–2507. https://doi.org/10.5194/bg-21-2493-2024

Thorson, J.T., Shelton, A.O., Ward, E.J., Skaug, H.J., 2015. Geostatistical delta-generalized linear mixed models improve precision for estimated abundance indices for West Coast groundfishes. ICES J. Mar. Sci. 72, 1297–1310. https://doi.org/10.1093/icesjms/fsu243

Walters, C.J., Pauly, D., Christensen, V., 1999. Ecospace: Prediction of Mesoscale Spatial Patterns in Trophic Relationships of Exploited Ecosystems, with Emphasis on the Impacts of Marine Protected Areas. Ecosystems 2, 539–554. https://doi.org/10.1007/s100219900101

Wells, B.K., Santora, J.A., 2023. Implementing an ecosystem oceanography program to increase capacity and preparedness for dynamic ocean management and fishery challenges. Front. Mar. Sci. 10, 1192052. https://doi.org/10.3389/fmars.2023.1192052

Zimmerman, M.S., Irvine, J.R., O'Neill, M., Anderson, J.H., Greene, C.M., Weinheimer, J., Trudel, M., Rawson, K., 2015. Spatial and Temporal Patterns in Smolt Survival of Wild and Hatchery Coho Salmon in the Salish Sea. Mar. Coast. Fish. 7, 116–134. https://doi.org/10.1080/19425120.2015.1012246

Tables

Table 1: Functional group summary table.

Model Group Code	Functional Group Short Name	Description / Characteristic Taxa
DE1-POC	Particulate organic carbon detritus	Represents pelagic suspended detritus as particulate organic carbon available for consumption by metazoans; Unconsumed DE1 flows to DE2
DE2-DOC	Dissolved organic carbon detritus	Represents pelagic dissolved organic carbon available for consumption primarily by microbes; Unconsumed DE2 flows to Export
PP1-DIA	Diatoms	Pennate and centric diatoms (e.g., *Skeletonema* spp., *Thalassiosira* spp., *Chaetoceros* spp.)
PP2-NAN	Nanophytoplankton	green algae (chlorophytes, prasinophytes), haptophytes / prymnesiophytes (e.g., coccolithophores; *Emiliania huxleyi*), golden algae (chrysophytes), raphidophytes (e.g., *Heterosigma* spp.), silicoflagellates (e.g., *Dictyocha speculum*), autotrophic nanoflagellates
PP3-PIC	Picophytoplankton	autotrophic prokaryotes, autotrophic eukaryotes, cyanobacteria (cyanophytes; e.g., *Synechococcus* spp.), small green algae (chlorophytes)
BA1-BAC	Bacteria	*Marinobacter*, *Alteromonas*, *Erythrobacter*
PZ1-CIL	Ciliates	heterotrophic and mixotrophic ciliates (Oligotrichida, Choreotrichida; aloricate; e.g. *Mesodinium rubrum*, *Strombidium* spp.), tintinnids
PZ2-DIN	Dinoflagellates	heterotrophic and mixotrophic dinoflagellates (e.g., *Gymnodinium* spp.)
PZ3-HNF	Heterotrophic Nanoflagellates	heterotrophic and mixotrophic nanoflagellates
ZF1-ICT	Ichthyoplankton	Pacific herring (*Clupea pallasii*), Pacific hake (*Merluccius productus*), smelts (*Bathylagus* spp., *Leuroglossus schmidti*), Northern anchovy (*Engraulis mordax*)
ZC1-EUP	Macro/Meso Crustacean Omnivores	Euphausiids (e.g., *Euphausia pacifica*, *Thysanoessa spinifera*, *T. inspinata*, *T. longipes*)
ZC2-AMP	Macro/Meso Crustacean Predators	Amphipods (e.g., *Cyphocaris challengeri*, *Themisto pacifica*)
ZC3-DEC	Meso Crustacean Meroplankters	planktonic early life stage decapods (e.g., *Cancer magister*);
ZC4-CLG	Meso Crustacean Herbivores	large copepods (e.g., *Neocalanus plumchrus*, *Eucalanus bungii*, *Calanus marshallae*)
ZC5-CSM	Meso/Micro Crustacean Herbivores/ Omnivores	small and medium copepods (e.g., *Metridia pacifica*, *Pseudocalanus* spp., *Paracalanus* spp.), Ostracods (*Discoconchoecia elegans*; *Conchoecia* spp.)
ZS1-JEL	Mega/Macro Gelatinous Carnivores	Scyphozoans (e.g., *Cyanea capillata*, *Aurelia aurita*); large hydrozoans (e.g., *Aequorea* spp.)
ZS2-CTH	Meso/Macro Gelatinous Carnivores	Ctenophores (Cydippids; e.g., *Pleurobrachia* spp.; i.e., comb jellies); small hydrozoans (e.g., *Aglantha digitale*, *Aegina* spp.)
ZS3-CHA	Meso Soft-Bodied Carnivores / Detritivores	Chaetognaths (i.e., arrow worms; e.g., *Parasagitta elegans*), Polychaetes (e.g., *Tomopteris septentrionalis*); pteropods and gastropods (e.g., *Limacina helicina* and *Clione limacina*)
ZS4-LAR	Meso Soft-Bodied Herbivores / Detritivores	Appendicularians (Larvaceans; e.g., *Oikopleura dioica*)
NK1-COH	Coho and Stream-type Chinook	Coho salmon (*Oncorhynchus kisutch*) and Chinook salmon (*O. tshawytscha*), stream-type
NK2-CHI	Ocean-type Chinook	Chinook salmon (O. tshawytscha), ocean-type
NK3-FOR	Small Forage Fish	Pacific herring *(Clupea pallasii),* Pacific sandlance (*Ammodytes hexapterus*), Northern anchovy *(Engraulis mordax),* eulachon *(Thaleichthys pacificus),* surf smelt *(Hypomesus pretiosus)*

Table 2: Basic Ecopath parameters: areal biomass (*B*), production (*P/B*), production-consumption ratio (*P/Q*), consumption (*Q/B*), and unassimilated consumption (*U*). Sources are provided in the Supplement.

Group	B (g C m^{-2})	P/B (yr^{-1})	P/Q	Q/B† (yr^{-1})	U
PP1-DIA	2.3	100	—	—	—
PP2-NAN	1.5	70	—	—	—
PP3-PIC	0.35	110	—	—	—
BA1-BAC	0.17	150	0.3	500.0	0.2
PZ1-CIL	1.1	90	0.35	257	0.22
PZ2-DIN	0.87	50	0.32	156.2	0.24
PZ3-HNF	0.46	70	0.55	127.3	0.2
ZF1-ICT	0.05	3.6	0.3	12.0	0.06
ZC1-EUP	0.60	5.76	0.28	20.6	0.18
ZC2-AMP	0.85	8.5	0.3	28.3	0.20
ZC3-DEC	0.18	7.5	0.26	28.8	0.40
ZC4-CLG	0.8	10.0	0.28	35.7	0.26
ZC5-CSM	1.00	16.0	0.28	57.1	0.24
ZS1-JEL	0.003	6.48	0.29	22.3	0.25
ZS2-CTH	0.03	19.8	0.32	61.9	0.25
ZS3-CHA	0.4	5.04	0.36	14.0	0.19
ZS4-LAR	0.05	88	0.33	266.7	0.25
NK1-COH	0.0046	6.1	0.28	21.8	0.2
NK2-CHI	0.00018	7.2	0.28	25.7	0.2
NK3-FOR	0.28	3.96	0.28	14.1	0.2

† The Q/B column was calculated for most groups from a P/Q estimate, as (P/B)/(P/Q).

Table 3: Main model setup and selected parameters of SOGEM-LTL. Parameters and settings are also available in the Supplement and model archive.

Category	Sub-Category or parameter	Adopted configuration
Setup	EwE formulation and workflow	Ecopath mass balance → Ecosim (non-spatial) → Ecospace (spatial, 2-D)
Resolution	Trophic aggregation / functional groups	22 groups: 3 primary producers; 1 bacterial; 3 protozooplankton; 4 soft-bodied zooplankton; 5 crustacean zooplankton; 1 larval; 3 nekton; 2 detrital groups
Resolution	Spatial / temporal resolution	~1.5 km horizontal grid; 120 time steps yr^{-1} (~3 days); 1980–2018 hindcast
Initial production	Primary-producer P/B (PP1 / PP2 / PP3)	100 / 70 / 110 yr^{-1}, respectively (Ecopath baseline)
Primary production	Maximum relative P/B (PP1 / PP2 / PP3)	20 / 20 / 20 (Ecosim Group Info)
Primary production	Ecosim production multipliers (PP1 / PP2 / PP3)	4.0 / 2.5 / 2.7 (non-spatial Ecosim configuration)

Irradiance	PP light-response right-point (PP1 / PP2 / PP3)	Ecosim: 24 / 20 / 23; Ecospace: 22 / 20 / 23 (right-shoulder response)
Temperature	PP temperature optima (PP1 / PP2 / PP3)	Ecosim: 11.8 / 14.0 / 15.0 °C; Ecospace: 11.8 / 14.5 / 15.0 °C
Nutrients	Initial fraction of generic nutrients free (p_{free})	0.51; single implicit nutrient pool partitions free / biomass-bound nutrient
Forcing	Physical forcing	HOTSSea v1 oceanographic fields and RDRS v2.1 atmosphe forcing; one-way offline coupling
Forcing	Vertical-resupply of nutrients – empirical proxy	Domain-mean mixing-layer depth (XLD) forcing; 22 m cap; day smoothing; mean-normalized to 1
Trophic dynamics	Foraging-arena vulnerability multipliers (γ)	1.4–2.0 in documented consumer–prey links; most near 2
Consumer responses	Ecosim Group Info max relative feeding time and max relative consumption settings	10 / 100 across consumer groups
Spatial movement	Ecospace dispersal and advection	Uniform base dispersal input across living groups (300 km yr advection and migration disabled
Initialization	Ecospace spin-up	50 model-years static/climatological forcing + 20 model-year using repeated 1980 forcing (EwE time scaling: 10 model-ye = 1 calendar year)

1073
1074

1075 Table 4: Table summarising data sources used for model evaluation.

Category	Description	Temporal Coverage	Source(s)
nutrients	Bottle-sampled nutrients (nitrogenous) from near-surface and 20 m depths	2012 - 2018	(Fisheries and Oceans Canada, 2025; Pacific Salmon Foundation (PSF), 2025)
bloom timing	Satellite derived estimates of spring bloom timing	2003 - 2016	(Suchy et al., 2022)
satellite chlorophyll a	1-km, 8-day MODIS-Aqua chlorophyll a composites (gap-filled) for the central SoG	2003 - 2016	(Suchy et al., 2022)
phytoplankton community composition and seasonal variability	Near surface phytoplankton community composition at northern SoG at Station QU39	2016 - 2018	(Del Bel Belluz, 2024; Del Bel Belluz et al., 2021)
phytoplankton	Seasonal biomass of phytoplankton and zooplankton	2015 - 2019	(McEwan et al., 2023)
zooplankton	Zooplankton biomass (seasonal)	1996 - 2018	(Fisheries and Oceans Canada, 2023; Perry et al., 2021)

1076 Table 5: Skill of SOGEM-LTL in reproducing spring bloom timing (day of year) in the central
1077 SoG against the satellite-derived series (2003–2016) and the C09 one-dimensional model series
1078 (1980–2018); the C09 series is also evaluated against the satellite series as a reference. N,
1079 number of years; R, Pearson correlation; Std. Ref. and Std. Model, standard deviations of the
1080 reference and model series (d); Bias, mean of model minus reference (d); MAE, mean absolute
1081 error (d); WSS, Willmott skill score; Categorical, years assigned to the same early, average or
1082 late class as the reference (satellite comparisons: day of year ≤ 68 and ≥ 108; C09 comparisons:
1083 mean ± 1 SD of the C09 series). Methods are given in Supplement Section S.3.3.

Comparison Source	SOGEM-LTL Module	N	R	Std. Ref.	Std. Model	Bias	MAE	WSS	Categorical
Satellite	Ecospace (2-D)	14	0.77	18.93	15.3	1.36	10.5	0.86	13/14 (93%)
Satellite	Ecosim (non-spatial)	14	0.65	18.93	12.46	-6.3	12.93	0.75	10/14 (71%)
Satellite	C09 1D model (reference)	14	0.77	18.93	10.84	1.5	11.1	0.80	11/14 (79%)
C09	Ecospace (2-D)	39	0.36	11.7	11.58	0.56	10.26	0.6	18/39 (46%)
C09	Ecosim (non-spatial)	39	0.38	11.7	10.61	0.41	9.6	0.61	17/39 (44%)

Figures

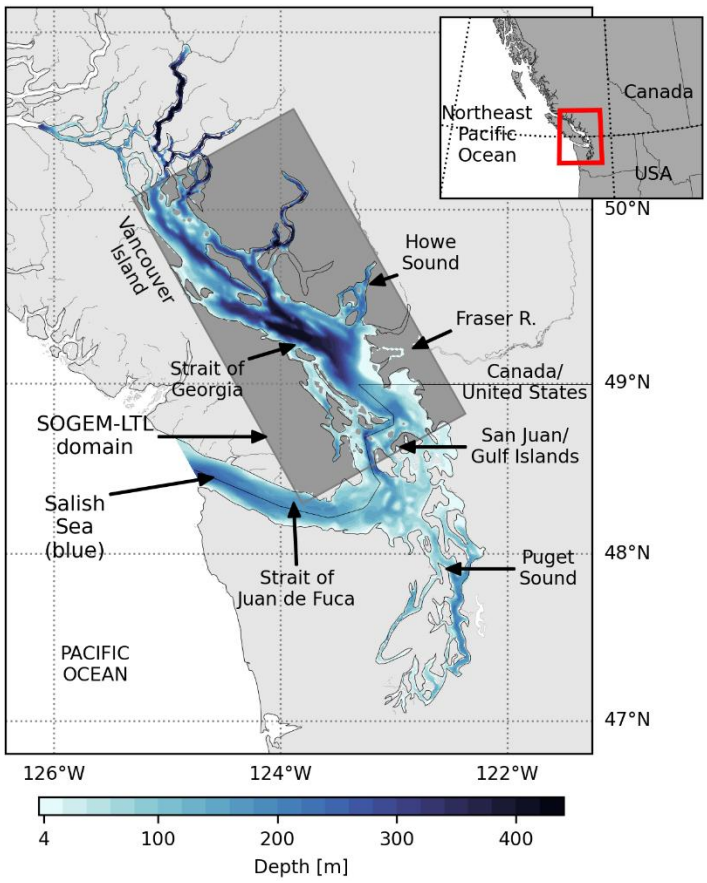


Figure 1: Map showing SOGEM-LTL model domain (dark grey) and the HOTSSea v1 model domain (light grey) covering the entirety of the Salish Sea (grey rectangle).

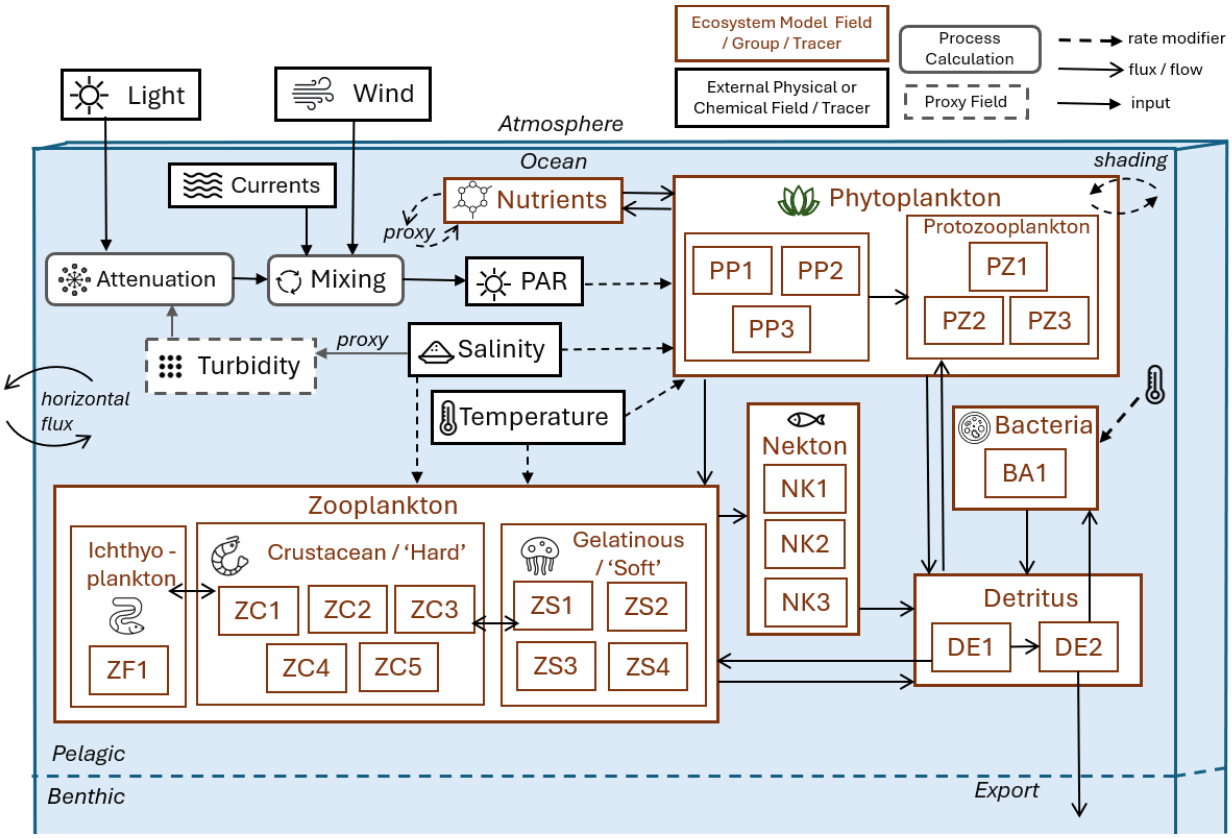


Figure 2: Conceptual illustration of the SOGEM-LTL model. See Table 1 and Table S2 for group code descriptions.

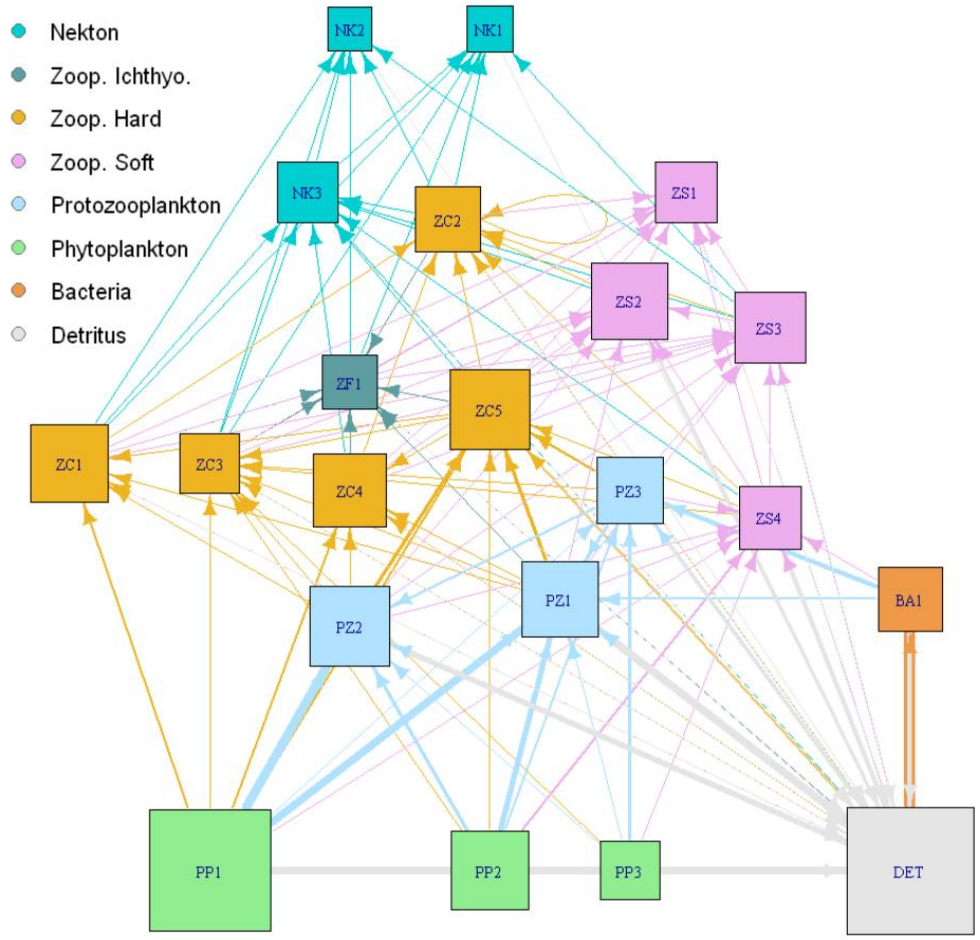


Figure 3: The food web representing the mass-balanced model arranged vertically by trophic level. Colours of boxes represent broad functional group categories and arrows point in the direction of biomass flow. The width of lines is proportional to total biomass flows (i.e., consumption) and the area of boxes are proportional to the total biomass of each functional group, re-scaled to permit visualisation of all groups.

1100

1101

1102

1103

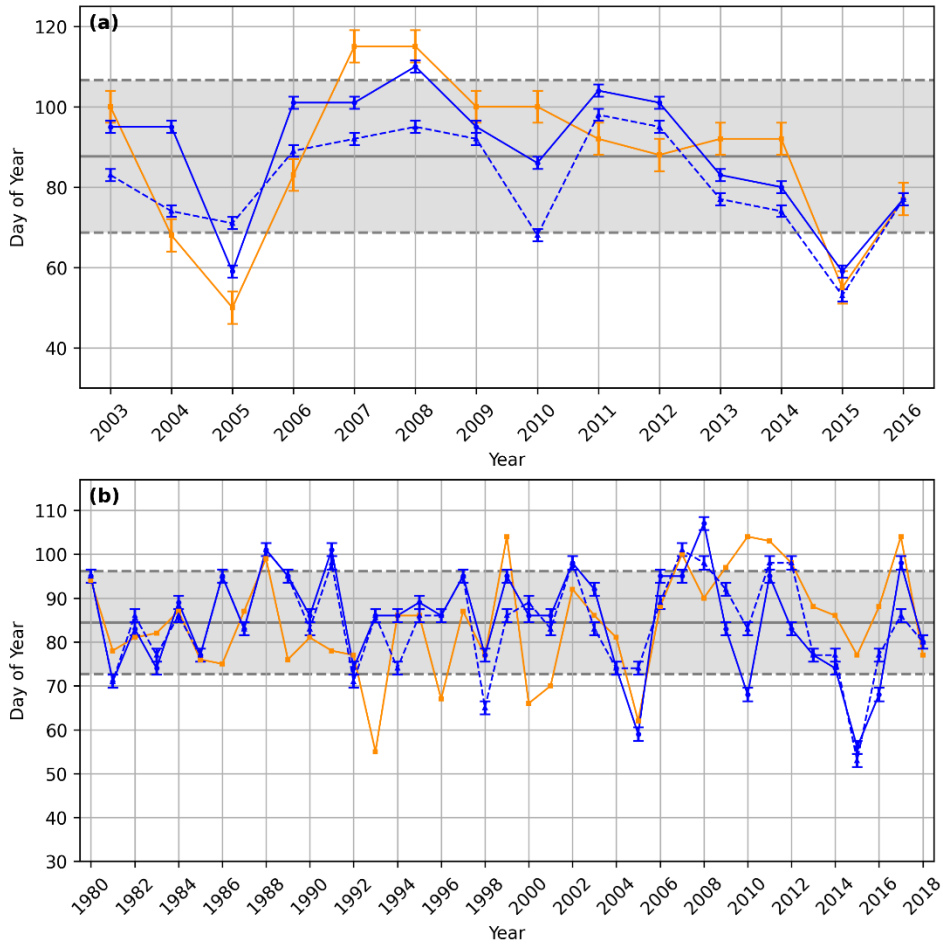


Figure 4: Spring bloom timing (day of year) in the central SoG from the SOGEM-LTL Ecospace (solid blue) and Ecosim (dashed blue) modules, compared with (a) satellite-derived estimates for 2003–2016 (Suchy et al., 2022) (orange) and (b) the C09 one-dimensional model for 1980–2018 (orange). Error bars represent ±1.5 days for the model and ±4 days for the satellite estimates. The grey line and band show the mean and ±1 standard deviation of each reference series (a: day 88; b: day 84). Early and late blooms follow the classification used for each reference: day ≤ 68 and ≥ 108 for the satellite series, and more than one standard deviation from the C09 mean (day ≤ 73 and ≥ 96) for C09.

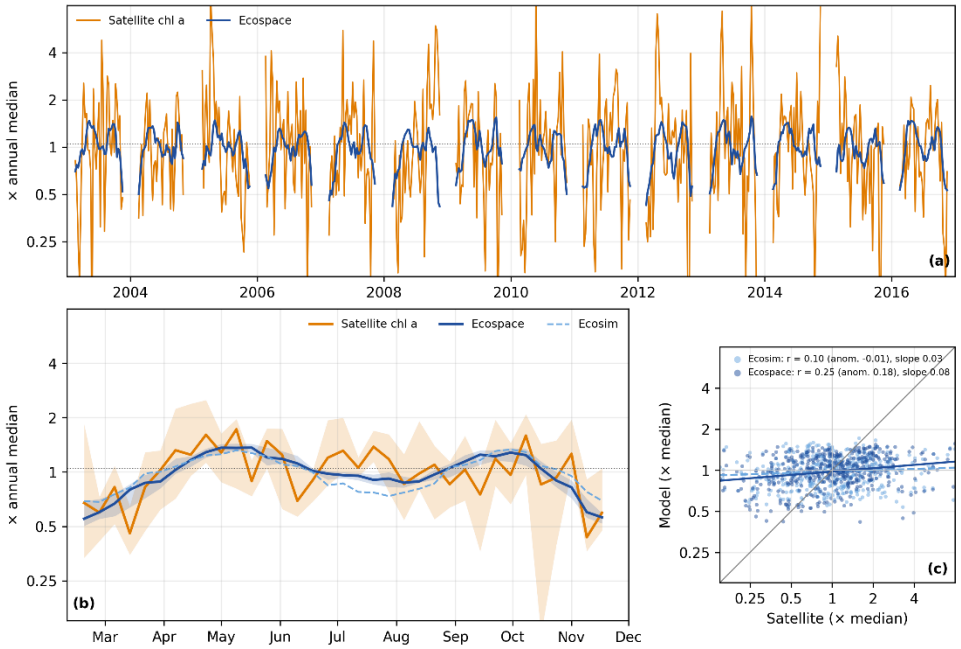


Figure 5: Central SoG phytoplankton relative to satellite chlorophyll a, 2003–2016: (a) 8-day MODIS-Aqua chlorophyll a (orange) and Ecospace phytoplankton biomass (blue); (b) median across years for each 8-day period (shading: interquartile range; dashed: Ecosim); (c) weekly model versus satellite values with log-scale fits. Values are relative to each series' seasonal median (Section S.3.3); dotted line: bloom threshold.

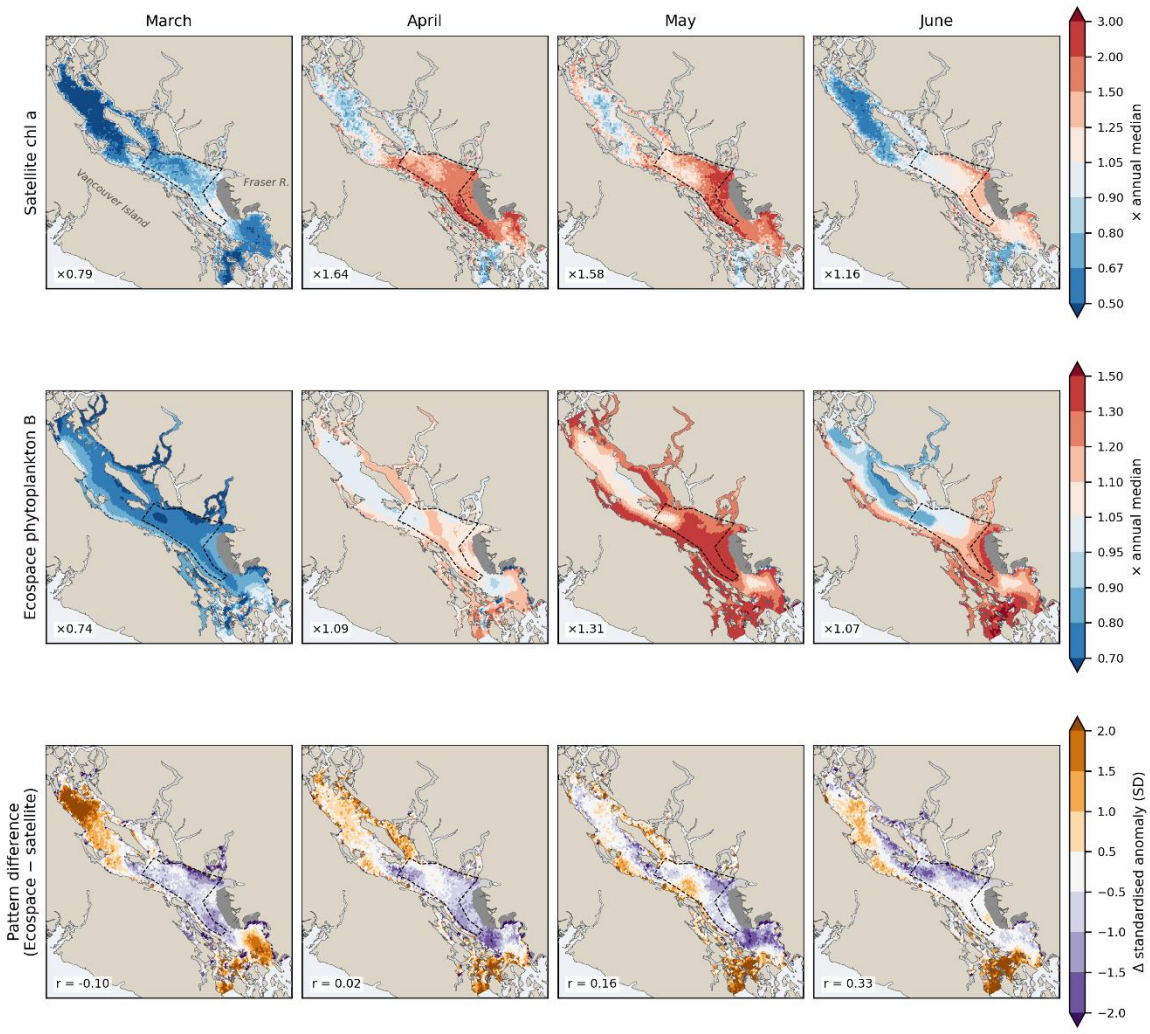


Figure 6: Monthly spring patterns, 2003–2016, relative to each source's seasonal median: (top) MODIS-Aqua chlorophyll a; (middle) Ecospace phytoplankton biomass; (bottom) difference between standardised spatial patterns (Ecospace − satellite). Rows have separate colour scales; numbers give the central SoG median (dashed region; top two rows) or the within-month spatial correlation (bottom row). Dark grey: Fraser River plume; light grey: no satellite data. Details in Section S.3.3.

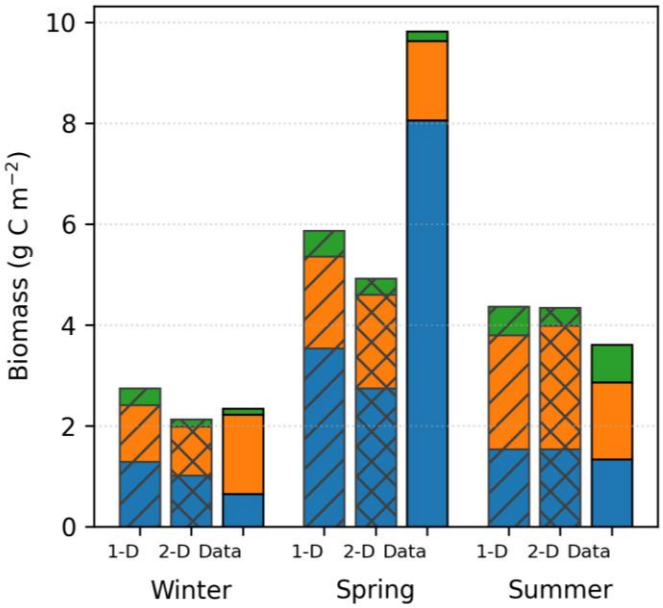


Figure 7: Seasonal mean absolute phytoplankton biomass from SOGEM-LTL non-spatial (Ecosim; diagonal lines) and spatial (Ecospace; hatched) modules versus estimates from field data compiled in a previous seasonal Ecopath model (McEwan et al., 2023). Diatoms (blue), nanophytoplankton (orange), and picophytoplankton / other (green) are compared by season.

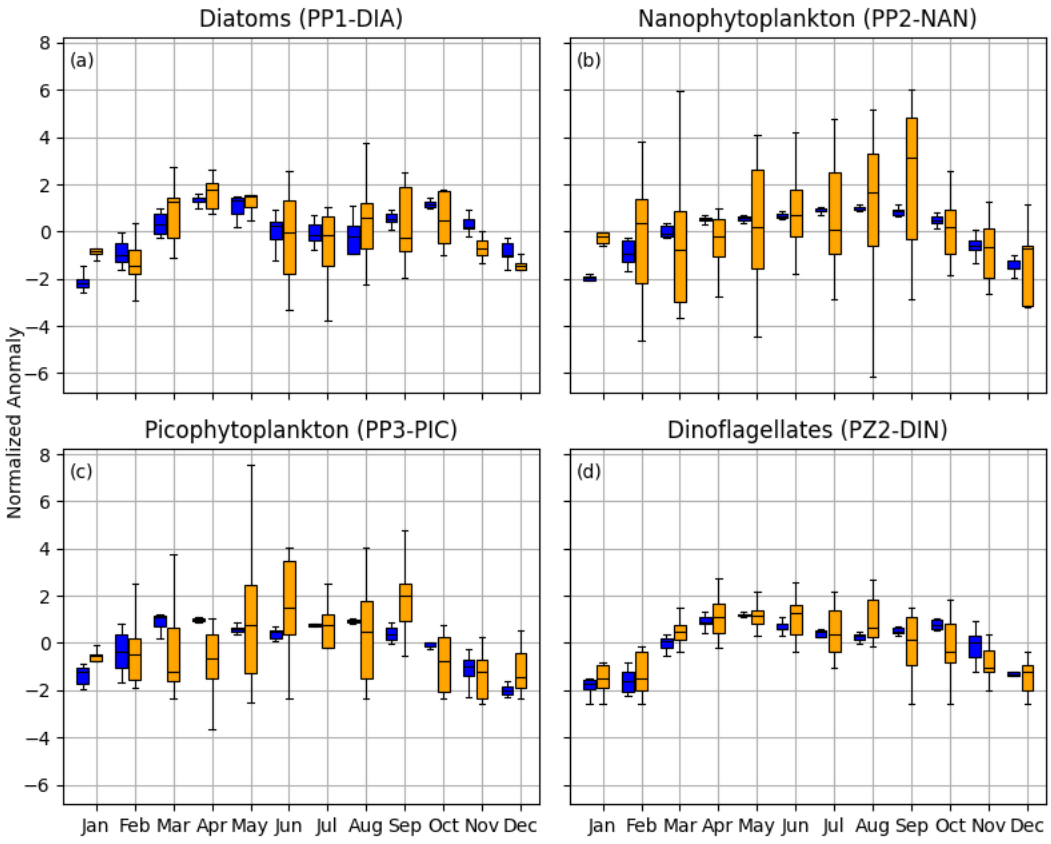


Figure 8: Monthly distributions of standardised departures from the annual mean (log-transformed) for SOGEM-LTL Ecospace (blue) and observations at station QU39 (orange) in the northern SoG, 2016–2018: (a) diatoms, (b) nanophytoplankton, (c) picophytoplankton (indicator taxon Pyramimonadophyceae) and (d) dinoflagellates. Observations are cell counts and model values are biomass, so each series is standardised separately.

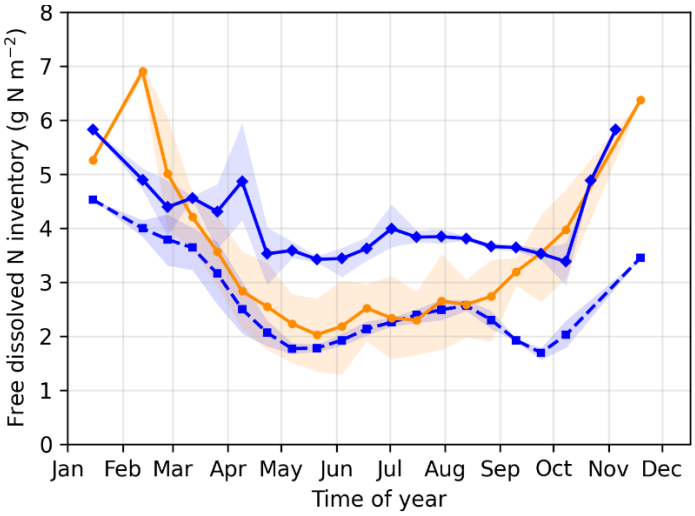


Figure 9: Biweekly climatology of surface-layer (0–20 m) dissolved inorganic nitrogen derived from field data (orange circles) and from matched SOGEM-LTL outputs, with Ecosim (dashed blue) and Ecospace (solid blue) results contrasted. Shading indicates the 10th–90th percentile across years.

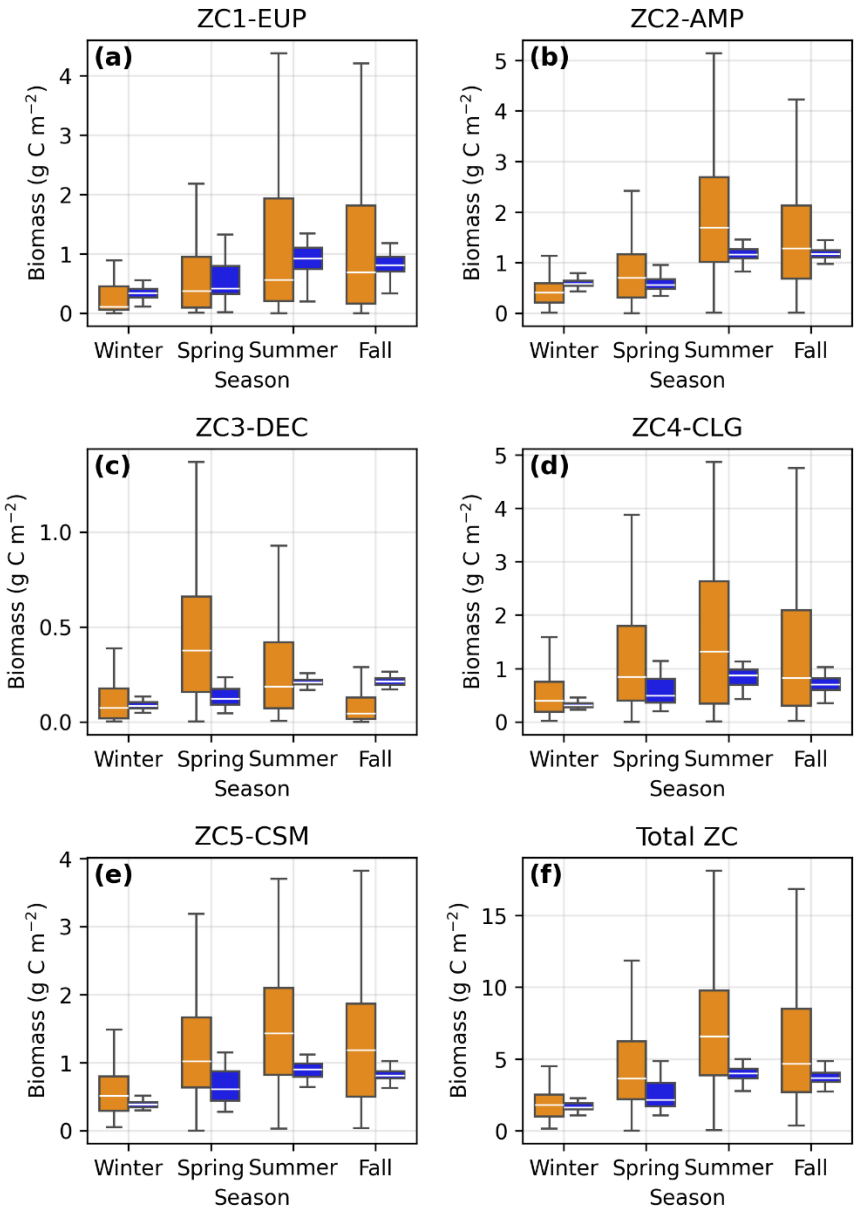


Figure 10: Seasonal boxplot panel of absolute biomass of crustacean zooplankton from the SOGEM-LTL Ecospace module matched to observations, shown by season for individual groups in panels (a)-(e) and for all crustacean groups taken together (f).